Journal of Electrostatics 119 (2022) 103735

Contents lists available at ScienceDirect

Journal of Electrostatics

journal homepage: www.elsevier.com/locate/elstat

A review of particle transport and separation by electrostatic traveling wave methods

Yue Yu [a,b], Jan Cilliers [b,*], Kathryn Hadler [b], Stanley Starr [b], Yanghua Wang [a,b,**]

[a] Resource Geophysics Academy, Imperial College London, South Kensington, London SW7 2BP, UK
[b] Department of Earth Science and Engineering, Imperial College London, South Kensington, London SW7 2AZ, UK

ARTICLE INFO

Keywords:
Dust mitigation
Electric curtain
Electro dynamic screen
Electrostatic traveling wave
Particle separation
Particle transport

ABSTRACT

The controlled movement of dry particles using non-mechanical means is desirable in a number of different applications, including solar panel dust mitigation, toner particle motion and in the handling and beneficiation of regolith for In-Situ Resource Utilization (ISRU). The electric curtain, the electrostatic traveling wave (ETW) and the electro-dynamic screen (EDS) are examples of techniques that can transport and separate particles with no moving parts nor fluid medium. This review paper brings together the research carried out on these techniques.

We provide a comprehensive review on the particle movement mechanisms and the development and application of ETW methods, featuring a diverse range of hardware and circuitry, particulate material and process objectives. We focus on the evaluation of experimental development in the area of dust mitigation, particle transport and ISRU processes. We also detail the current knowledge about theory and modelling methods. Moreover, we provide a guide for possible improvement of the effectiveness of ETW devices, by outlining the limitations in application, theoretical understanding and potential research aspects.

1. Introduction

An electrostatic traveling wave (ETW) field can be produced by parallel electrodes and a suitable multiphase voltage source. Neutral or charged fine particles brought into such a field will move with different trajectories due to the action of the electric force, gravitational force, and other forces related to their different physical properties. Some particles may be charged further by contact with the dielectric layer covering the electrodes (tribocharging). Electrostatic traveling wave systems with appropriately designed parameters, such as electrode configuration, interspacing and voltage characteristics, can be used to transport and separate fine dry particles.

1.1. ETW and electrostatic standing wave

An ETW transport system consists of a flat insulating surface with embedded linear electrodes. The voltage applied to these electrodes generates an electric field. If a single phase or two-phase time-varying voltage is applied to the electrodes, a standing wave is generated. When using multiple-phase voltages, a traveling wave can be produced. Fig. 1 shows a schematic of the ETW hardware and the electric field.

1.2. Particle transport mechanisms

When a neutral or charged particle enters into a non-uniform electric field (e.g. circular electrodes), electric charges will be redistributed at the surface of the particle. Positive and negative charge will accumulate on opposite sides of the particle, producing dipole polarity. This results in a dielectrophoretic (DEP) force and particle movement [1].

The triboelectric effect produces electrostatic charge exchanges on particles through rubbing, both between particles and between particles and the surface of the dielectric layer. The exchange of charge depends on the work functions and surface physical properties of the materials in contact. Particles will accumulate charges on them via tribocharging as they move along the surface of the dielectric layer covering the electrodes [2]. Particles with a net charge due to this effect are affected by Coulomb forces which are typically stronger than DEP force.

The basic charge transfer between two dielectric materials and mechanism of tribocharging is poorly understood [3,4], because the actual charge transfer behaviour depends on multiple factors, including

* Corresponding author. Department of Earth Science and Engineering, Imperial College London, South Kensington, London SW7 2BP, UK.
** Corresponding author. Resource Geophysics Academy, Imperial College London, South Kensington, London SW7 2BP, UK.
E-mail addresses: yy2120@ic.ac.uk (Y. Yu), j.j.cilliers@imperial.ac.uk (J. Cilliers), kathryn.hadler@list.lu (K. Hadler), s.starr@imperial.ac.uk (S. Starr), yanghua.wang@imperial.ac.uk (Y. Wang).

https://doi.org/10.1016/j.elstat.2022.103735
Received 8 April 2022; Received in revised form 15 June 2022; Accepted 1 July 2022

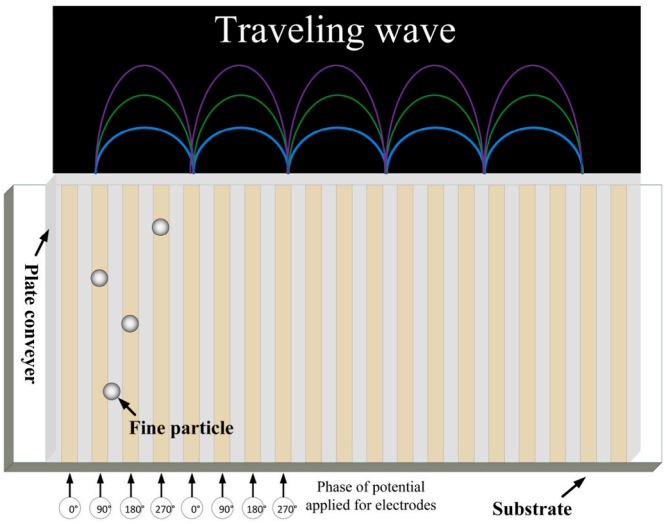

Fig. 1. Schematic of particle movement platform with an ETW field, a plan view of the electrodes and an elevation view of a conceptual electrostatic wave.

the nature of contact, environmental conditions such as temperature and humidity, and any surface processing history [5,6]. Basic concepts and theories of charge transfer, as well as experimental and simulation methods, can be found in review papers [7,8], and will not be discussed further here.

1.3. Particle motion modes

The particle moving mode in ETW field depends on the experimental conditions. The moving trajectories of particles can be classified into different modes. By changing frequencies of applied voltage (varied from 10^{-1} to 10 Hz), Masuda observed five motion modes, shown in Fig. 2 [9]. At the lowest frequency, particles will drop onto the surface and bounce alternatively, shown as (a) in Fig. 2, called stepwise motion. As the frequency rises, particles will not drop, but move with a constant velocity, Fig. 2 (b), called forward motion with constant velocity, as the electric force and resistance on the particle are in balance. If the frequency rises further, particles move in a circular motion (c), and the direction may be forward or backward. Particle motion (d) has a smaller velocity with higher circular frequency than (c). At even higher frequency, particles will spin (e) with a very small average horizontal velocity. This vibration mode was also observed in Kawamoto's experiments [10].

Melcher at al. [11] used a dimensionless model to analyze the particle average moving speed analytically and compared it with numerical results under single-phase perfect traveling sinusoidal wave. The particle motion was classified into two modes depending on the particle average velocity: synchronous- and asynchronous mode. In synchronous mode particles have similar average velocities to that of the traveling wave, while in asynchronous mode particles have much smaller average velocities than the traveling wave. Melcher at al. [11] studied particle motion analytically, and generated similar motion to Fig. 2 (a), which they termed hopping mode, a synchronous mode. Melcher at al. Further proved that particles in cyclic motion (Fig. 2 c and d) could only have low velocities, called curtain mode, an asynchronous mode, and that it is likely when the frequency is greater than the key frequency $f = \sqrt{gk}/\pi$, where g is a normalized parameter and $k = 2\pi/wavelength$.

Further to Masuda and Melcher's work, Schmidlin [12] put forward another transport mode, called surfing mode, in which particles slide or roll along the conveyor surface. Surfing mode is used in the transport of toner particle for electrophotography. Schmidlin suggested that large particle adhesion force may transfer motion from hopping mode to surfing mode.

Summarizing and unifying the usage of different terminologies, we conclude that particle motion in an ETW field can be classified into four different modes:

1) Curtain mode: Particle moves in a cyclic motion with small average velocity
2) Hopping mode: Particle drops onto the surface and bounces forward or backward
3) Surfing mode: Particle slide or roll along the conveyor surface
4) Vibration mode: Particle spins with very small average velocity

Note that particles can move forward or backward in hopping mode.

1.4. Terminology

The earliest concept using traveling electrostatic force to remove charged particles on the plate was put forward by NASA [13] in a report

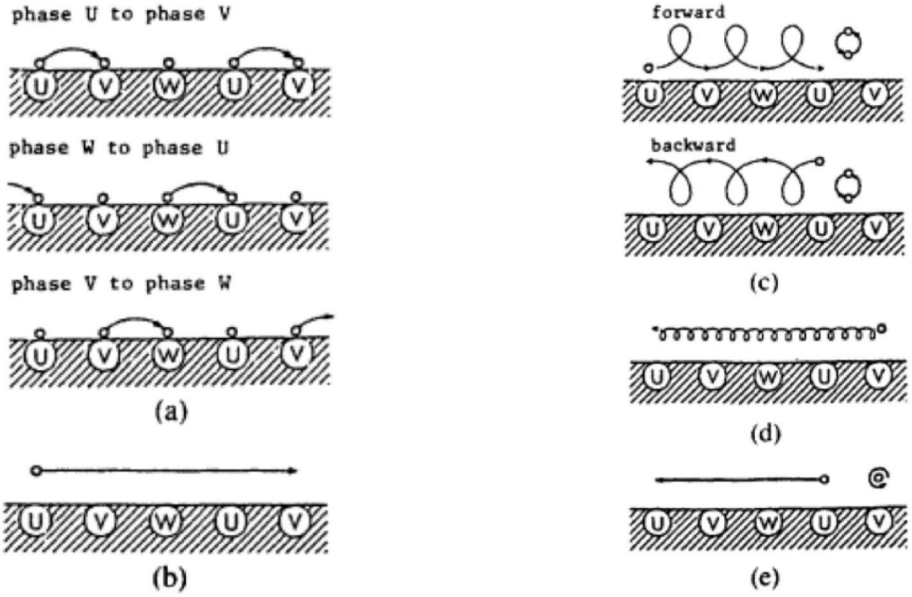

Fig. 2. Particle's motion modes under different frequencies of voltage [9].

of various means of clearing dust from thermal radiator panels on the Moon. The test platform is shown in Fig. 3 and the brush is a charged conducting rod isolated by an insulation layer. In this design the charged conductor is mechanically swept across the surface using the same apparatus used to test a mechanical brush. According to the report (13, section 3.5.6) time and funding limitations did not allow testing of the electric brush. Instead basalt particles were charged and dropped onto the plate or the plate was charged, both tests in the laboratory atmosphere (other concepts were tested at high vacuum). The removal of dust was not effective and only some of fines particles could fly away [13]. The report provides insufficient data and detail to analyze its lack of performance.

Compared with the type of single electrode proposed by NASA, type of parallel cylinder electrodes was first introduced by Masuda and co-workers, shown in Fig. 4 [14]. Single phase and multiple phase voltages were applied to electrodes, and charged particles entering into this field could move effectively under the action of the electric- and other forces.

The electrodynamic screen (EDS) uses a similar configuration of electrodes and variable electric fields, as shown in Fig. 5. EDS is typically used for dust mitigation, for example on solar panels [15].

This paper provides a comprehensive review of the particle movement in an ETW field, introduces the development and application of ETW methods and identifies research gaps. The experimental platforms of the electric curtain, EDS and ETW are very similar. Further, as will be shown, these technologies use the same theory, similar electric field calculation methods, and particle motion simulation methods. The electric curtain and EDS are therefore included in this review. In the following sections, ETW will refer to the basic theory and be used as a general term for the physical method, while electric curtain and EDS will refer specifically to their industrial applications.

A schematic (Fig. 6) summarises the applications of the electric curtain, EDS and the controlled movement of particles using ETW.

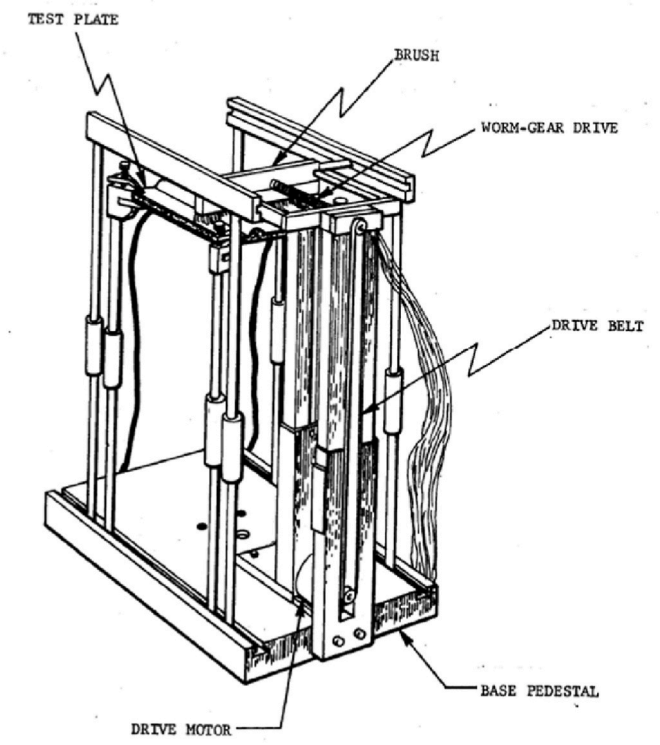

Fig. 3. Final design of electrostatic concept of dust removel test platform [13].

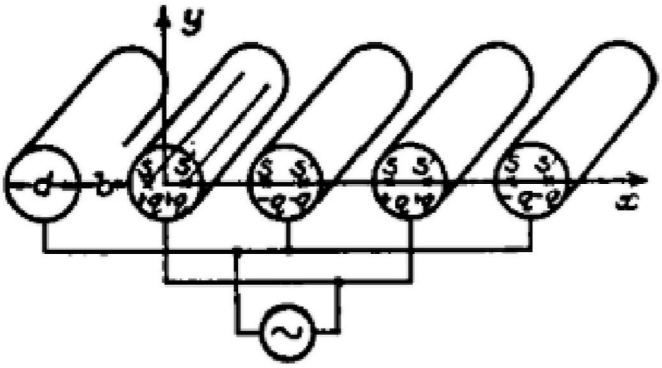

Fig. 4. Electric curtain [14].

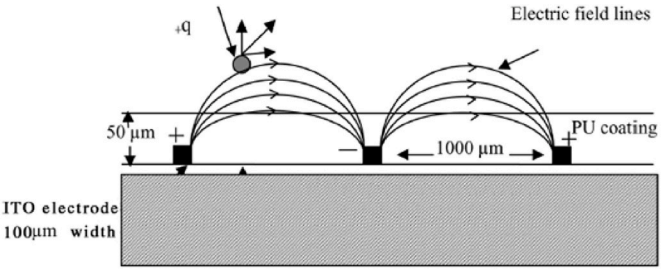

Fig. 5. Cross profile of EDS system [15].

1.5. Literature classification

Previous research applications can be divided into three categories: dust mitigation, particle transport and particle separation, shown in Table 1. Within the three categories, we further classify particle transport and separation according to particle type, and classify dust mitigation systems further according to usage conditions and environments. Table 1 makes explicit links between different research areas that use the same ETW methods and research directions.

Considering the complexity of particle motion analysis in an ETW field and the diverse applications of the ETW method, direct comparison between the experimental parameters and results and theoretical research are scarce. There remains many fundamental theoretical aspects of ETW that are unexplored, rendering further development and implementation challenging.

This review has four sections: Section 1 gives a comprehensive introduction to ETW methods, particle transport modes and applications. In section 2, the evolution of different ETW methods is reviewed. In section 3, theoretical research and experimental methods in particle transport and separation are critically examined and their potential and limitations discussed. In section 4, research gaps are identified and the review summarises.

2. ETW systems development

This section describes the development of ETW equipment designs and their performance at laboratory and industrial scale.

2.1. Electric curtain

The early work of Tatom et al. [13] and Masuda at al [14, 66, 104]. was developed further [9, 66, 81], with a focus on practical application, systematic theory and experimental methods. The first application aimed to transport charged aerosols in a spatially periodic, non-uniform field [66]. Charged aerosol particles move mainly by gravitation, and electric force can be used to confine their trajectories. The research

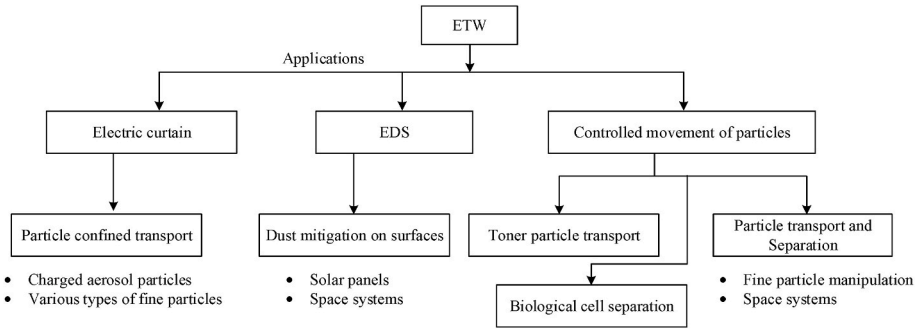

Fig. 6. Schematic of application areas.

Table 1
References classified by different applications and objectives.

Application		Objective of study	Reference
Dust mitigation	Solar panels on Earth	Comprehensive research on mechanism and performance analysis of dust mitigation	[2,15–33]
		Particle trajectories simulation on solar panels	[34–39]
		Effect of particle size on dust mitigation	[40–43]
		Effect of humidity on dust mitigation	[44]
		Force analysis on dust mitigation processes	[1,45]
	Mars conditions	Experimental research	[46–51]
	Moon	Experimental research and simulation	[52–58]
	Mars and Moon	Exploration of dust mitigation	[18,48,59,60]
Particle transport	Fine particle	Mechanism of particle transport, experimentally and by simulation	[10–12,61–73]
	Toner particle	Demonstrate controlled motion of toner particles, experimentally and by simulation	[74–82]
	Lunar soil	Experimental research and simulation	[83,84]
	Sample of asteroid soil	Experimental research	[85–87]
	Metal pieces (copper, bronze and steel)	Experimental research	[88,89]
Particle separation	Biological cell separation	Calculation of electric field and DEP force analysis	[9,90–95]
		Cell movement research: experiment and simulation	[9,96]
	Fine particle separation	Platform design research for particle separation	[97–101]
	Lunar particle separation	Demonstrate lunar particle separation experimentally and by simulation	[102,103]

investigated electrode types (Fig. 7) and voltage phases, and demonstrated flexibility in handling charged particles. Using a non-uniform traveling wave field, Masuda at al. [96] explored biological applications by moving cells in a fluid. Different electrode types and configurations were tested to protect cells from damage during transport and separation, and to improve the efficacy [9, 96]. In lower area near electrodes, harmonic component of traveling wave field became more dominant. Due to the action of harmonic waves, heavier or less charged cells near the electrodes moved backward, which could be utilized for cell separation. Two types of two-wave component systems were developed to research the effects of harmonic waves [96]. One type was constructed by superposing two different waves, three-phase and six-phase waves, on the electrodes simultaneously, and the other type was constructed by two electrode arrays paralleled with a space. The results showed that moving direction of cells was related to the distance between cells and electrodes, where the proportion of harmonic component was different. This proved the effect of harmonic waves on moving direction of cells.

Subsequent efforts were made to understand the observations quantitatively and to design improved test devices for charged particles. First, Yen and Hendricks designed a double electric curtain to trap specific particles from air flow with either gravity or air drag, as shown in Fig. 8 [82]. Melcher et al. [61, 62] combined a numerical model and dimensional analysis to explore the theory of particle movement in an ETW field applied with six-phase voltage. It was found that the frequency of applied voltage is the predominant factor determining the particle moving mode [62].

Comprehensive analyses of the effects of viscous drag, particle mass, gravity- and electric fields [11], and numerical simulations were used to improve the performance of a charged toner transport device [61]. Schmidlin [81] subsequently developed a new xerographic system that can transport toner particles vertically. It was found that these particles may ‘flock’ together and move along with the traveling wave.

The phenomenon that particles moving backward under certain conditions has been utilized to separate biological cells [9, 96] and agricultural seed by-products [105]. These papers explained that the backward motion was due to the harmonic waves in the field. Schmidlin [12] revisited the particle motion modes using numerical analysis, claiming that the reason for backward motions may be more likely due to the space charge and collision between particles with conveyer surface than the effect of harmonic waves. Backward transport in simulation using single pure wave may be an artifact of large incremental time steps. Therefore, the backward movement of a single particle in a fluid observed experimentally [9] still couldn’t be explained thoroughly [12]. Recently, Zouaghi and Zouzou [27, 34] have analysed the effect of harmonic waves using numerical results, which suggested the backward motions were due to harmonic waves. However, the backward trajectories shown in their papers were in the hopping mode and included contacting with conveyer, so the effect of collision between particles and conveyer may also contribute to the backward motion. This question needs attention.

Lycopodium particle’s oscillatory behaviour in plane type electric curtains has been researched in detail by Dudzicz [106–109]. Particles entering the electric curtain were observed to move in four ways: 1) oscillate near electrodes steadily; 2) oscillate above and below the curtain; 3) slow down near electrodes or leave the curtain; 4) travel from one electrode to another. The space above the electrodes was classified into two regions according to the angle of vibration path related to the center of electrodes, designated separation region and saddle region. In the separation region, particle’s oscillation path changed significantly with small change of charge. While in the saddle region, particles moved more stable and were more easily confined [106]. Using the region of

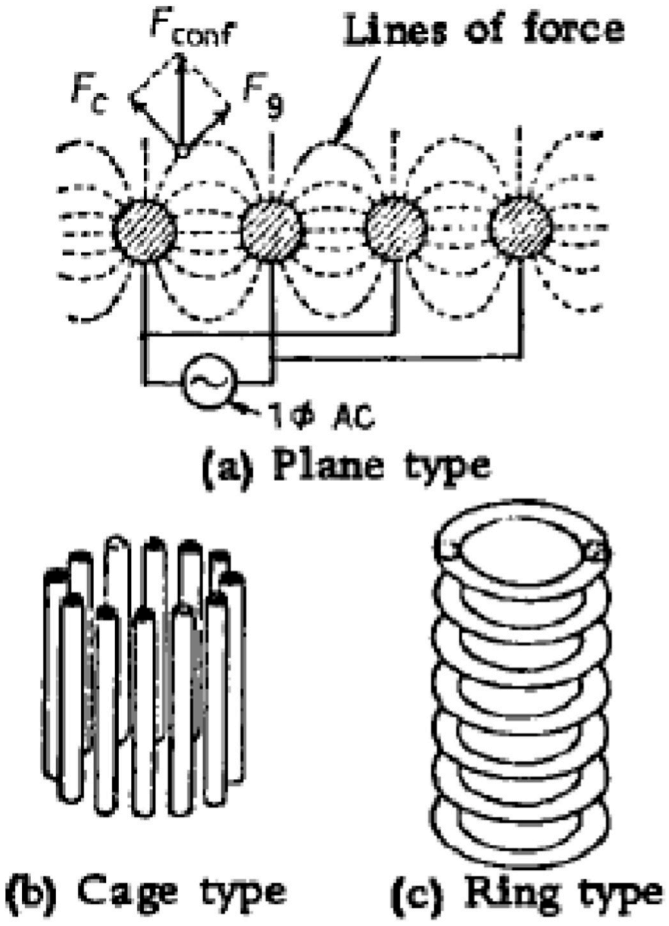

Fig. 7. Principle and basic constructions of electric curtain [66].

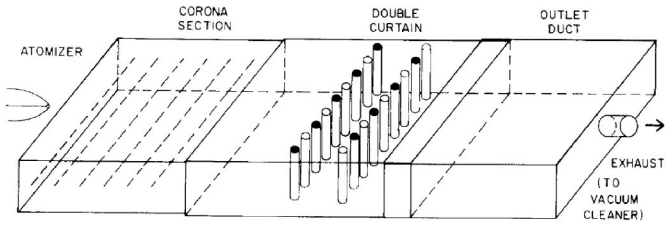

Fig. 8. Particle trap double curtain system. Bars with different coloured ends have opposite polarities [82].

separation, particles with target of charge could be separated according to their different trajectories [107]. The frequency of applied voltage had a large influence on the position of two regions. The range of frequency 20–80 Hz was the best for dust precipitation and particle separation [108]. A DC voltage has been added to the electrodes to create hybrid-type electric curtain, which provides more options to control particle's trajectory [109].

2.2. Dust mitigation (EDS)

EDS, using AC electric fields, has been widely studied for dust mitigation systems, particularly on solar panels. Experimental platform and typical configurations are shown in Figs. 9 and 10.

Experimental investigation and numerical simulation of dust mitigation used on Earth or in space has received increasing attention and has been conducted by many researchers, notably the group of Calle at the NASA Kennedy Space Center [18, 19, 48, 49, 56, 59, 60], the group

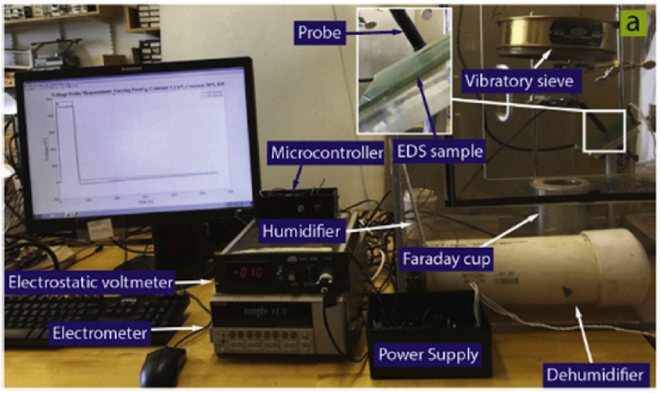

Fig. 9. Experimental platform of EDS system [30].

Fig. 10. Field test of EDS system in Saudi Arabia [25].

of Mazumder in the University of Arkansas at Little Rock [2, 15, 20, 22, 26, 31, 32, 41], the group in Qian Xuesen laboratory of space Technology, China Academy of Space Technology [64, 65], the group of Kawamoto in the University of Waseda [16, 47, 52–54], the group of Noureddine in the University of Poitiers [27, 34, 45, 67], the group of Guo in Texas A&M University [28, 29, 33, 36, 44], and the group of Amar in Djillali Liabes University of Sidi-Bel-Abbes [43, 89]. The research and findings are classified into following sections.

2.2.1. Terrestrial conditions

1) Effect of particle size and electrodes configuration

Johnson at al. [42] and Biris at al. [17] researched the effect of particle size and particle charge on dust removal efficiency (DRE), which was defined as the percentage of dust removed from the initial amount of dust on the screen. The electrode voltage was set as a 5 Hz square wave with amplitude ranging from 6 to 7 kV. Two JSC Mars-1 dust simulants were tested. The DRE for the coarser dust (5.8 μm median size, 14–20 μm more abundant) was significantly higher than for the finer dust (5.2 μm median size, 0–5 μm particles more abundant). Increasing the electrodes spacing from 1.26 mm to 2.54 mm reduced the DRE. However, pre-tribocharged particles were removed more efficiently with 1.26 mm than 2.54 mm electrode spacing. The combined effect of voltage frequency cannot be omitted. The experimental results by Ahmed and coworkers [43] showed that for Polyvinyl Chloride (PVC) particles: 1) if the particle's size is 90 μm, the frequency of voltage at 33 Hz and spacing at 0.5 mm is the optimal design; 2) if the particle's size is 125 μm, the frequency of voltage at 15 Hz and spacing at 1.0 mm is the optimal design; And they used MODDE. 05 program to estimate that if particle's size is at 250 μm, the frequency of voltage at 10 Hz and spacing at 0.8825 mm will be the optimal design.

Sayyah et al. [41] included the effect of particle size distribution on the loss of energy from sunlight. Electrode width was 80 μm and inter-electrode spacing varied from 400 μm to 800 μm, by 100 μm increments. The duty cycle of applied voltage was 50%, the voltage amplitude 1 or 1.5 kV and the frequency 5 Hz. The particle size distribution on the screen showed that higher voltages removed more and smaller particles. In addition, increasing the screen tilt angle improved dust removal performance. If the angle was larger than or equal to 40-°, interelectrode spacing had little effect on dust removal. Through analysing forces on different size of particles, Zouaghi and coworkers [45] found that the efficiency of EDS decreased with the increase of particle size due to the larger gravitational force on them.

Research on the movement mechanisms for different sizes of particles is reviewed in section 3.2, which is helpful for the design of EDS.

2) Effect of humidity and charge to mass ratio (Q/M)

The particles charge state affects the performance of the system. In most terrestrial applications, particles are initially neutral and the forces exerted by the ETW are due to DEP force. As the particles contact the dielectric layer and each other, they may become tribocharged. In the lunar environment with high vacuum, UV radiation, solar wind and zero humidity, particles are likely to have an initial charge [110]. Unfortunately, few ETW studies have measured or reported the charge state of particles.

Kawamoto et al. [10] measured the charge of initially neutral particles (density about 3.5 kg/m^3 and size from 30 μm–110 μm) transported on a ETW conveyor, covered with acetate rayon film (3M, 810-18D), using a Faraday cage and free-fall. They found that particles were charged to −0.01 to −0.03 μC/g by contacting with the surface of the dielectric layer. The charge distribution evolved over time into two peaks, explained by tribocharging between particles. They further compared the charge density as a function of particle size and found that surface charge density on small particles, especially smaller than 40 μm, is higher than on large particles due to the ratio of superficial area to mass [102].

Sayyah et al. [30] investigated how electrode width, spacing, voltage type and relative humidity affect the Q/M of particles in an EDS system. Particles used in the experiments were JSC Mars-1A simulant dust and sized by an 88 μm vibratory sieve. Electrodes were covered with a two stacked layer, optically clear adhesive film and borosilicate glass with relative permittivity of 5.14 and 5.5, respectively. Their measurements showed that a decrease in voltage and an increase in electrode width and spacing decreases the magnitude of electric field on the surface of screen, thus decreasing the Q/M of the particles.

Zouaghi and Zouzou [27] measured the charge of 50–300 μm spherical PMMA particles after moving on an ETW conveyor made of epoxy resin reinforced with fiberglass (relative permittivity: 4.3). The results showed that particles were mainly charged positively with a Q/M of several 0.01 μC/g.

Javed and Guo considered the effect of relative humidity on EDS performance, which showed that performance decreased significantly with increasing humidity [44].

In general, a larger Q/M led to higher clearing factor. However, measurements of charge-to-mass ratios indicated that the Q/M of Mars dust simulant, which had the highest clearing factor, was the smallest while the Q/M of lactose was the highest [17]. This demonstrates that other particle characteristics will affect their movement on the screen. The effect of material properties remains to be studied in greater detail.

3) Effect of dust deposition modes

Guo et al. [36] studied EDS performance under aerosol- and sieve deposition and various operation cycles. Aerosol deposition of dust is more realistic than sieve deposition [16]. The median diameter of the airborne dust was about 20 μm with a mean density of 78 mg/cm^3. A single square wave with frequency of 1 Hz and peak-to-peak value of 6 kV was applied to electrodes with width of 0.3 mm and pitch of 7 mm, covered by a 55 μm dielectric layer. Sieve deposited dust was easier to remove than aerosol deposited. Under single operation mode, a low rate of dust loading led to a decrease in DRE. Moreover, in cyclic-operation, with new dust loaded on the surface after each single operation, a certain amount of dust tended to be kept on the screen in each cycle in aerosol deposition mode, which led to a continuous decrease of DRE with more cycles, while dust removal efficiency of sieve deposition mode was less affected by the number of cycles.

4) Effect of characteristics of traveling wave

Experimental system by Biris at al. [17] had 0.762 mm thick electrodes with a 1.524 mm gap between electrodes and the applied voltage was 10 kV at a frequency of 300 Hz. It was found that DRE increased linearly with an increase in voltage and varied little with frequency, which only affected the speed of removal. In addition, DRE decreased from pulse-to square-to sinusoidal applied waveforms. And tests of DRE of three dust types found that the Mars dust simulant was the easiest to clear, followed by acrylic powder, and finally lactose. Similar conclusions were obtained in Refs. [16, 99] that square wave was more effective than sinusoidal and triangular wave, because square wave has a higher root-mean-square (RMS) amplitude than the other two waves with same peak value.

Since EDS can be regarded as a capacitance load, the charging time to peak wave can be adjusted by input current, resistance and the load of capacitance, which was proved to have effect on the efficiency of EDS by Guo and coworkers [33]. They found that the efficiency of EDS in the condition of low rise time of voltage (100 ms–6 kV_{pp}) dropped by 50% compared with fast rise time in cyclic operation mode [36]. The decreasing effect on EDS efficiency of rising time was also interfered by deposition mode and dust loading level in single operation mode.

5) Evaluation of energy cost

Sharma et al. [51] researched the energy cost of EDS relative to DRE. It was estimated that the average power for an EDS system was 0.017 mW/cm^2 to 0.049 mW/cm^2. If the width and spacing between electrodes was set to 127 μm and 508 μm respectively, dust removal efficiency could remain above 90% and dust accumulated on the surface of screen would not exceed 0.64 mg/cm^2. However, adding an electrode layer on the solar panels led to a 15% power output drop.

6) Outdoor field test

EDS outdoor field testing has been conducted by Faes at al. [25] in Saudi Arabia and Guo at al. [29] at Doha, Qatar, which revealed a difference between indoor and outdoor tests. Faes and coworkers [25] have found that different dust deposition rates had a significant effect on the capability of the EDS system. The highest DRE could reach 95%, however, the DRE may drop to 10% at relative higher dust loading density. Future designs of EDS need to consider local environmental conditions.

Guo and coworker [29] developed metrics of cleaning index (CI), Cleaning Index Change Rate (CICR) and soiling loss (SL) to better evaluate dust removal efficiency for the outdoor test of EDS. Three photovoltaic modules, active EDS, inactive EDS and reference model without EDS electrodes, were tested in same conditions to make comparison. The electrodes of EDS were designed to 0.3 mm width and 7 mm pitch, and were applied to two-phase square wave, which was a low cost fabricated way compared with three- or four-phase wave. They found that this type of EDS could reduce loss by 16%–33% with the activation voltage of EDS at 9 kV_{pp}, while at 6 kV_{pp}, the efficiency of EDS was zero. The data collected related to weather conditions like wind and rainfall were shown to have a significant effect on EDS efficiency.

Sayyah et al. [21] compared the restoration of reflectivity of solar panels after cleaning by different methods: EDS, natural cleaning by rain and snowfall and manual cleaning by water and detergent. It showed that: the cleaning effect of natural rainfall on solar panels was related to the angle of inclination and surface glazing material. This report [31] showed that manual water washing cleaning could restore 98% of the original reflectivity, while EDS restored more than 90% reflectivity.

Guo and coworker [28] have also performed four-days short term field tests of EDS using outdoor soiling microscopy (OSM) method. The micrograph image of dust on EDS surface were used to quantify particles and their behaviour. It revealed that particles close to electrodes could be removed more successfully in the beginning stage of field test, and this position dependent phenomenon weakened with the increase of test time. In addition, particles that stayed longer on the surface were harder to remove, which may due to the increasing adhesion force. The proportion of dust mass removed by EDS decreased from 40% to 14% in the four days test averagely.

2.2.2. Martian and lunar conditions

1) Test of Martian condition

Calle et al. [49, 60] researched the performance of an electrodynamic dust shield system under simulated Martian atmosphere conditions of 0.93 kPa CO_2. Concerning the electrical breakdown at low atmospheric pressure, the amplitude of voltage applied to electrodes was lower than 800 V [49]. Even though the electric field strength was not high in the test, the EDS performed extremely well with continuously activation because the lower atmospheric pressure and dry conditions decreased the required electrostatic forces for particle movement. Experiments of dust clearing performance of thermal radiators on spacecraft have been conducted under similar experimental conditions and the results indicated that DRE can reach up to 99% with 50 mg of 50–100 μm sized JSC-1A dust delivered to each 10 cm × 16.7 cm dust shield [60].

Atten and coworker [50] tested the performance of dust removal in air and CO_2 atmosphere with different level of pressure, respectively, using a standing wave field. Certain applied voltages on electrodes could generate dielectric barrier discharges (DBDs) in the gas, which was found to be helpful to charge particles and improve particle removal efficiency. Under low pressure conditions, the design of the electric curtain should have a high ratio of the applied voltage for DBD and the distance between electrodes. This generates larger electric field to overcome the influence of strong adhering force.

2) Effect of electrode configuration

In Calle et al. [60], the experiments were conducted under three electrode width and spacing configurations: width and spacing between electrodes set to a) 0.6 mm and 2.0 mm; b) 0.5 mm and 1.5 mm; c) 0.3 mm and 1.0 mm, respectively. The effect of electrode configuration is complex since increasing the width will enlarge the magnitude of the electric field while increasing spacing has the opposite effect. The minimum voltage amplitude required for particle transport decreased linearly as the frequency decreased and it was lowest in the configuration of b, followed by a, and highest in c.

Detailed research about the effect of electrodes configuration was also conducted by Calle et al. [48]. It showed that increasing the spacing between electrodes decreased the clearing factor and this effect was most obvious in the Martian atmosphere at 0.4 kV. When electrode width varied from 0.3 to 0.4 mm, the four types of electrode pitch (sum of width and space between electrodes), set at 0.48 mm, 0.55 mm, 0.6 mm, 0.67 mm, respectively, could recover the output voltage of solar panels to above 90% after activating the system in lunar conditions at high vacuum [56, 59].

3) Effect of wave type and frequency

Dust simulant of Mars JSC-1, lunar JSC-1a, and Minnesota simulant were tested under Martian and lunar conditions [48]. Operating frequency had no effect on DRE at 1.5 kV and little effect at 0.4 kV. In addition, it was proved that a sinusoidal traveling wave contributes more to the rolling of particles and a square wave contributes more to the lift of particles.

4) Dust removal for spacesuit

Kavya and coworkers [57] have researched the possibility of dust removal from lunar spacesuits using EDS. Yarns made of Carbon Nanotube (CNT) flexible fibers were used to make electrodes for EDS, which has exceptional mechanical and conductive properties suitable for spacesuit conditions. CNT fibers were embedded into “orthofabric” material to test its performance. CNT fibers diameters were 200–215 μm with two types of spacing between electrodes, 1 mm and 1.6 mm. The results showed that EDS could efficiently repel nearly 90% of dust dropped to surface and 80%–95% of dust deposited on the surface in advance. In addition, the work function matching coating (WFM) created by ion beam sputter deposition with a similar work function as the lunar simulant was added to the surface to test DRE. This showed very similar performance with uncoated EDS. The advantage of WFM was that it could be used as passive precipitation technology by reducing electrostatic adhesive force on dust particles. A more complete SPacesuit Integrated Carbon nanotube Dust Ejection/Removal (SPIcDER) system was developed on the knee part of spacesuit [58]. In the scaled test, only 4–16% of area remained uncleaned and the increase of voltage showed increased cleaning efficiency. A safety risk analysis in the operation of this system addressed in four risk areas: 1) human exposure to CNT material; 2) hazardous electric fields; 3) electric arcing; 4) oxygen rich atmosphere.

2.3. More controlled particle movement

2.3.1. Particle transport and separation on earth

Machowski and coworkers [100] performed experimental and simulation research to separate particles using three-phase traveling waves. The traveling wave field was composed of harmonic waves. If the second harmonic wave was large enough, it could move particle in the opposite direction of basic traveling wave. Different types of particles could be separated by moving in different direction. Cylindrical and stripe electrodes with different widths and pitches were tested, while the type of triangle electrodes was not suitable due to low second harmonic

wave strength. Sand and pulverised alumina powders with mean diameter 192 μm and 40 μm were used. The results showed that particles could be separated in two frequency bands. At lower frequency, sand particles were transported followed the direction of traveling wave, while alumina particles were transported in the opposite direction, and both of them were in hopping mode. At higher frequency, Their movement direction reversed. Small particle alumina powder flew higher in curtain mode in the direction of traveling wave and sand moved slowly in the opposite direction in hopping mode. In addition, conveyers with higher ratio of electrode width to pitch had a higher separation efficiency.

This same group studied the transport of cohesive [98], lactose powder (150 mesh), which were successfully transported if the applied voltage exceeded 3.5 kV_{pp} with the frequency from 40 to 130 Hz.

2.3.2. Application to in-situ resource utilization

The electrostatic traveling wave methods have received significant attention in the area of In-situ Resource Utilization (ISRU), which refers to the use of natural resources from space, such as the Moon and Mars [111]. ISRU can produce fuel and consumables to reduce terrestrial launch mass and dependency in deep space missions [112]. ISRU has gaining importance in recent years, such as in the Exploration Technology and Development Program (ETDP) led by NASA in 2005 [113] through to the more recent Mars Oxygen ISRU experiment (MOXIE) [114].

Successful implementation of ISRU mining technology requires a complete process with stages of excavation, beneficiation, and extraction [115]. Beneficiation reduces the raw regolith to a feedstock enriched in the appropriate material for the subsequent process steps. The first beneficiation stage is the separation of particles by size. It has been shown that ETW methods can be used for lunar mineral beneficiation through size separation of regolith particles [83]. The group of Kawamoto at Waseda University, Japan have made significant contributions to the application and theory development of particle separation and transport with ETW using both experimental and simulation methods [10, 53, 68,83, 85–87, 97, 116]. Their experimental research is introduced in this section and their simulation method will be introduced in section 3.

To simulate the Moon, experiments were conducted on the system in vacuum as shown in Fig. 11 [102]. In this experimental platform, the conveyor was composed of parallel copper electrodes (thickness 18 μm, width is 0.3 mm and interspace 1.0 mm) and a polyimide cover (thickness 0.1 mm, width 128 mm, and length 490 mm). The applied voltage was a four-phase square wave and its amplitude was 1 kV. Different sizes of lunar regolith simulant FJS-1 particles (diameter 10–100 μm) were fed onto the conveyor. Particles floated and moved along the conveyor at different altitudes and could be collected at different heights above the conveyor. The charge density on small particles was larger and they moved higher. Particle separation was not successful under Earth ambient conditions due to air drag force [97]. However, in vacuum, particles with diameters smaller than 20 μm could be separated effectively. Moreover, simulations indicated that particles would lift higher under vacuum, so the collection box needs to set higher than the same condition on the Earth. The yield of specific particles was not given [83, 102], and needs to be verified in future studies.

Vertical transport for lunar regolith and ice particles have been researched with the application of mining lunar icy regolith [84]. The schematic view and experimental photograph are shown in Fig. 12. A four-phase square wave was applied to ring electrodes around the tube. Effects of the pitch of the electrodes, the distance between the end of tube with sample surface, the tube diameter, voltage amplitude and voltage frequency on particle transport rate were researched. The threshold for insulation breakdown was 4.6 kVpp, so 4 kVpp was selected. The test results showed that the optimal frequency was 30 Hz, and the optimal pitch and inner diameter of tube was 5 mm and 10 mm, respectively. The transport rate of 100 mg/min can be achieved in a 1-m-long tube. Numerical simulation under Lunar conditions using discrete element method (DEM) indicated this system could have an even higher performance due to low gravity and the absence of air drag. A similar vertical transport system [103] can be used to separate particles less than 10 μm with a lower applied voltage, like 1.0 kVpp. In this system, gravitational force on larger particles predominated, keeping larger particles toward the bottom. The average size of collected particles was 12 μm and 30% of them were smaller than 10 μm in the box placed at higher platform using a four-phase 10 Hz square wave and a vibrated particle supplier.

3. Theory and modeling

Development of the ETW method has evolved mostly along a “trial and error” approach in choosing operating parameters such as voltage type, electrode configuration and the insulating layer. The ETW has been applied in a wide range of fields including toner transport in electrophotography [81], dust mitigation on solar panels [2], space devices [60], and lunar soil particle transport and separation [13, 102]. A theoretical analysis of particle forces [1,45] and how particles move in the ETW field will allow for the optimal design and selection of critical parameters in these conveyor systems, particularly for manipulating the behaviour of particles of different sizes and composition.

3.1. Electric field calculation

3.1.1. Analytical method

Detailed knowledge of the potential distribution of the electric field in ETW systems is required to predict particle trajectories. Calculations assume a static electric field because the changes in the field due to

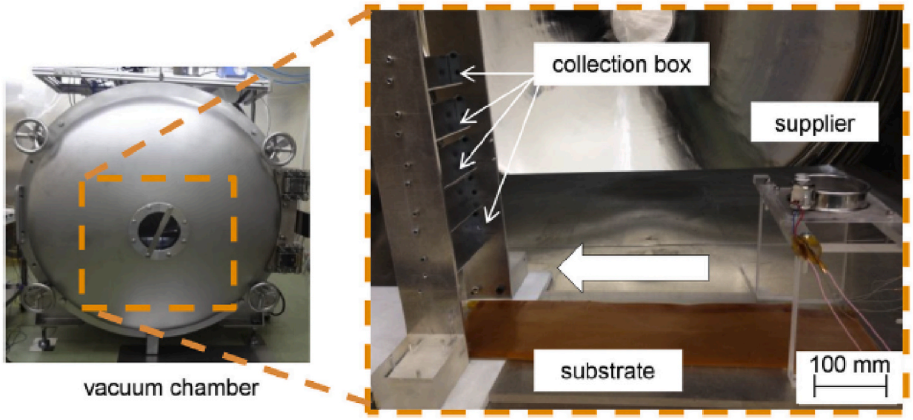

Fig. 11. Photographs of experimental set up in vacuum chamber [102].

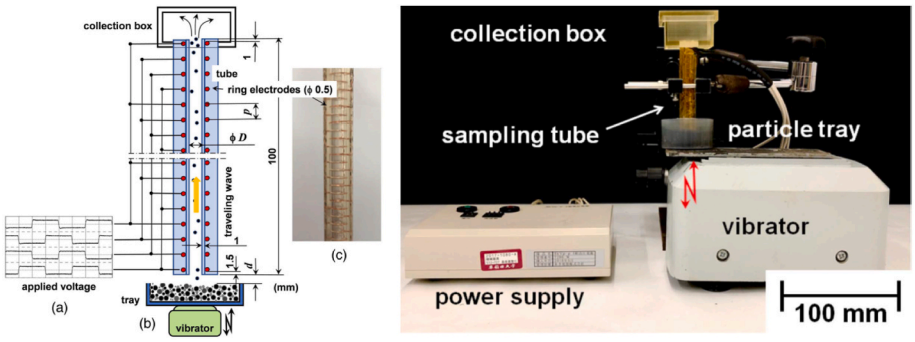

(a) schematica view (b) realistic experiment platform

Fig. 12. Vertical transport of lunar regolith and ice particles using ETW [84].

switching the polarity of electrodes is very rapid compared to the time they are constant when the applied voltage is square wave. Table 2 summarises the calculation methods applied in the literature to calculate the electric field for parallel electrodes where the DEP force is the predominant force in the manipulation of particles.

The diagram for the calculation model is shown in Fig. 13. Generally, the length of the electrode is much larger than the width and pitch, so the variation of the gradient of electric field in the y direction is treated as zero. In addition, the height of particle transport is also much smaller compared with the size of the electrode array. Therefore, the electric field in the y direction is thought to be uniform and the electric field potential distribution can be converted to a two-dimensional problem.

The basic form for this two-dimensional electrostatic problem is expressed as Laplace's equation with boundary conditions (1):

$$\begin{cases} \dfrac{\partial^2\varphi(x,z)}{\partial x^2}+\dfrac{\partial^2\varphi(x,z)}{\partial z^2}=0, \\ \varphi(x,z)=V_1, \quad \text{on the surface of electrode I,} \\ \varphi(x,z)=V_2, \quad \text{on the surface of electrode II,} \\ \varphi(x,z)=V_3, \quad \text{on the surface of electrode III,} \\ \varphi(x,z)=V_4, \quad \text{on the surface of electrode IV,} \\ \cdots \end{cases} \tag{1}$$

V_1, V_2, V_3, etc. represent the surface potential of each electrode. The voltages usually cycle with a fixed phase difference. Additional boundary conditions are provided by the potential falling to zero at infinity in x and z. The electric field is obtained by calculating the gradient of potential: $\boldsymbol{E} = -\nabla\varphi$.

An example of the distribution of potential and electric field intensity above the electrodes are shown in Fig. 14 and Fig. 15. Fig. 14 is a contour plot of potential above the electrodes and Fig. 15 is a stream plot of the electric field above the electrodes. This electric field is calculated with four electrodes by the charge simulation method and the potentials

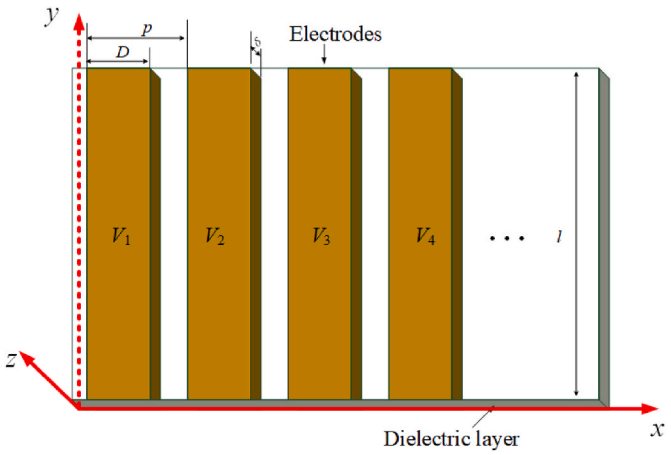

Fig. 13. Diagram showing the typical application system, consisting of the interdigitated electrode array. D is the electrode width, p is the electrode pitch, and δ is the electrode thickness, l is the electrode length. V_1, V_2, V_3, etc. Represents the surface potential of each electrode.

on the four electrodes are 800V, 800V, −800V, −800V, respectively. The black bars on the bottom of the two figures indicate the position of four electrodes.

Masuda and Kamimura [104] modelled the ETW field by introducing two first-order approximation methods and a more accurate approximation, the substitute-charge method, and compared the results. Then, they expanded the results using a Fourier series approach and found that the first and second modes play the predominant role. Finally, they compared the results of the three methods and showed that the application of two kinds of the first-order approximation methods becomes justifiable in the region X/λ ≥ 0.5–1.0 (X: height of calculation space, λ: wave length of the traveling wave).

Table 2
Review of electric field calculations (twDEP (traveling wave dielectrophoresis)).

Electrode type/configuration	Field wave	Dielectric Layer on top	Force analysis	Calculation method	Comparing Method	Reference
Cylindrical	Traveling	No	No	Substitute charge method	Traveling plane charge Approximation	[104]
Line (neglecting thickness)	Traveling	No	DEP force	Green' theorem	Charge density method	[90]
Bar (neglecting thickness)	Standing And traveling	No	DEP force twDEP force	Fourier series	Experiment	[91]
Bar (neglecting thickness)	Standing And traveling	No	DEP force twDEP force	FEM Solver FlexPDE	Fourier series	[92]
Bar (neglecting thickness) With lid	Standing And traveling	No	DEP force twDEP force	Schwarz-Christoffel mapping method.	Fourier series FEM (COMSOL)	[94]
Top and bottom electrodes	Standing	No	DEP force	Fourier series	FEM (COMSOL)	[95]

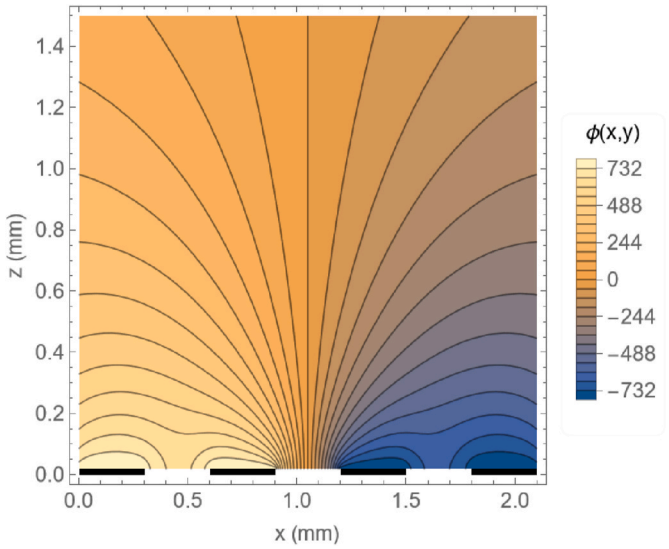

Fig. 14. Contour plot of potential above electrodes.

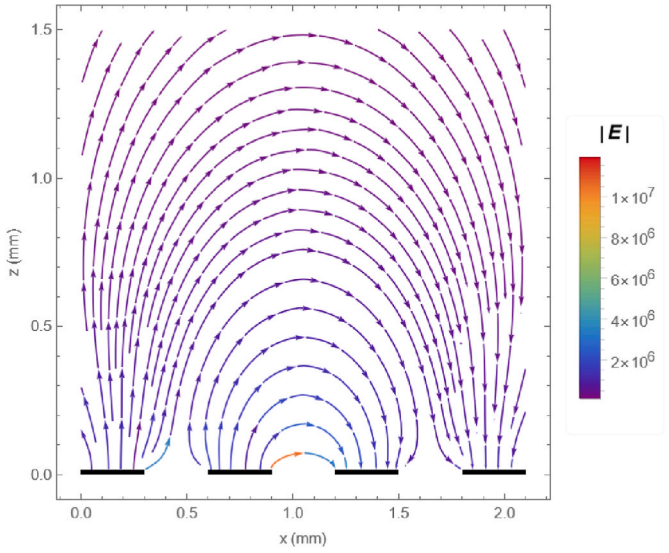

Fig. 15. Stream plot of electric field above electrodes.

In a later study, Wang et al. [90] used Green's theorem to calculate the electric field for two-dimensional electrode arrays, which can be used for the sorting and separation of biological cells. The Green's theorem approach to the solution of Lapalce's equation can be stated in integral form using Green's second identity, as follows:

$$\int_V dV\left(\varphi\nabla^2\psi - \psi\nabla^2\varphi\right) = \oint_A dA\left(\varphi\frac{\partial\psi}{\partial n} - \psi\frac{\partial\varphi}{\partial n}\right). \tag{2}$$

Here φ and ψ represent any two continuous scalar functions; n represents the unit normal vector; dV and dA represent an infinitesimal volume and infinitesimal area respectively. φ can be set as the potential function that needs to be solved. In order to choose a suitable Green's function, they ignored the thickness of electrodes and assumed an infinite number of infinitely long electrodes are arranged in a horizontal plane. In addition, they made the approximation that the potential varies linearly with distance across the electrode gap. In this way, the function of ψ can be deduced by a mirror-image method:

$$\psi = \frac{q}{|r - r_0|} + \frac{-q}{|r - r_0^{'}|}, \tag{3}$$

where q represents a point charge, and $|r - r_0|$ represents the distance between the calculating point and the point charge, and $|r - r_0^{'}|$ represents the distance between the calculating point and the mirror position of the point charge. The potential function related to r can be calculated as:

$$\varphi(r_0) = -\frac{1}{4\pi q}\oint_A \varphi\frac{\partial\psi}{\partial n}dA. \tag{4}$$

They also provided a method to eliminate the approximation of linear potential variation between electrodes by assuming a homogenous dielectric material with a zero normal field component in the electrode gaps. With this boundary condition, they calculated the polynomial coefficients of the Taylor expansions of electric potential in the electrode gaps. The relative RMS error for the electrical potentials are 1.1% at the calculation height, the same quantity with electrode width and 3.6% at the surface of electrodes for the third-order polynomial. They compared their results for the potential distribution at a height $z = 10$ μm with the charge density method and the difference is mostly immediately above the electrode, as can be expected [90].

Morgan et al. [91, 92] developed two methods for calculating DEP force in electrostatic traveling fields. They first used the Fourier series of the potential function, equation (5), to meet the boundary conditions. The potential between the electrodes is assumed to vary linearly, as in Ref. [90].

$$\varphi(x,z) = \sum_{n=1}^{\infty} A_n \,\mathrm{Cos}(k_n x)e^{-k_n z}, \qquad z > 0, \tag{5}$$

where A_n represents Fourier coefficients and $k_\mathrm{n} = 2\pi\mathrm{n}/\lambda$, where n is an integer, and λ is the wavelength. The A_n can be solved using the condition, $z = 0$ at the electrode plane. Note that equation (5) is the general solution to Lapalace's equation for the space above the electrode plane. Morgan et al. [91] compared the results of levitation height between their equation and experiments, finding deviations from 2.5% to 15%. Green et al. [92] specified the boundary conditions of the real and imaginary parts (φ_R *and* φ_I) of the potential function at the center vertical boundary line of electrodes, equation (6), and the boundary conditions cycled within the whole domain:

$$\begin{cases} \varphi_R = 0, \\ \dfrac{\partial\varphi_I}{\partial n} = 0, \end{cases} \quad \begin{cases} \varphi_I = 0, \\ \dfrac{\partial\varphi_R}{\partial n} = 0, \end{cases} \quad \cdots \tag{6}$$

They used a finite element solver to get a numerical solution. They found a derivation between the FEM and Fourier series methods of as much as 13%. By changing the FEM boundary condition to that of Morgan et al. [91], the differences were reduced to 0.013%.

Sun et al. [94] provided an analytical solution for these parallel electrode arrays and boundary conditions. The Schwarz-Christoffel Mapping Method was used to tackle the equations in the complex plane and they obtained the final expression in terms of Jacobian elliptic functions. However, in their calculation, they ignored the thickness of electrodes.

Gauthier et al. [95] developed a Fourier series method to calculate DEP force with two facing electrode arrays. However, they can only calculate the electric field with a given potential on the electrodes and the errors tend to be about 20% compared with FEM.

3.1.2. *Finite element method (FEM)*

The COMSOL Multiphysics software has been used widely to analyze the potential and electric field distributions under complicated ETW structures using the FEM [37, 55, 117]. The advantage of FEM is that designers can change parameters at will. Through analysing the electric field of ETW systems with different parameters, such as electrode configurations and types of dielectric layer, they can qualitatively analyze

how these parameters affect particles moving in such a system. However, the calculation accuracy of the finite element method is closely related to the scale of mesh divisions, so proper mesh patterns need to be designed. For instance, at the edge of the electrodes and the dielectric layer where the potential is changing rapidly, the size needs to be divided extremely finely, while further away from the electrodes it can be coarser [22]. The finite element results are, however, difficult to apply to predict the trajectory of a particle in motion.

3.2. Particle movement research

A theoretical understanding of the electric field distribution and how particles are transported in the ETW system will help to select relevant parameters in future applications such as a lunar regolith transport system. The forces affecting particle motion include the Coulomb force ($\boldsymbol{F}_C$), DEP force ($\boldsymbol{F}_{dep}$), gravitational force ($\boldsymbol{F}_g$), friction force, image force ($\boldsymbol{F}_{image}$) and air drag force ($\boldsymbol{F}_{drag}$) and any other forces which may be relevant in the particular case (Fig. 16).

The Coulomb force experienced by a particle will consist of the sum of the electric field intensity $\boldsymbol{E}_0$ generated by electrodes and $\boldsymbol{Eq}$ created by other charged particles [10]. Therefore, the electric field $\boldsymbol{E}$ at certain point can be obtained by

$$\boldsymbol{E} = \boldsymbol{E}_0 + \boldsymbol{E}_q = -\nabla\varphi + \frac{1}{4\pi\varepsilon_0}\sum_{n\neq i}^{N} q_N \frac{\boldsymbol{r}}{|r|^3}, \tag{7}$$

where ε_0 is the vacuum permittivity, N is the total number of particles in the field, q_N is the charge on a particular particle and $\boldsymbol{r}$ represent the distance between calculating point with nth particle: $\boldsymbol{r} = (x_i - x_n, y_i - y_n, z_i - z_n)$. The Coulomb force on a particle is given by

$$\boldsymbol{F}_C = \boldsymbol{E}\cdot q. \tag{8}$$

The air drag on a spherical particle can be calculated as follows [34]:

$$\boldsymbol{F}_{drag} = 6\pi\eta R\cdot(\boldsymbol{U}_g - \boldsymbol{v}_p)\cdot\frac{1}{C_U(R,\lambda_g)}, \tag{9}$$

where η is the viscosity of air, R is the particle radius, $\boldsymbol{U}_g$ is the flow velocity, $\boldsymbol{v}_p$ is the velocity of the particle, Cunningham factor C_U is related to the radius of particle and mean free path of the gas molecules, λ_g. Since the research referenced here takes place in air at atmospheric pressure, C_U can be assumed to equal 1, because R is several orders of magnitude larger than λ_g.

The DEP force on a single particle generated by the non-uniform electric field acts on the induced dipole moment of particles and can be expressed as [118]

$$\boldsymbol{F}_{dep} = 4\pi R^3\varepsilon_0\varepsilon_m\frac{\varepsilon_p - \varepsilon_m}{\varepsilon_p + 2\varepsilon_m}\boldsymbol{E}_0\nabla\boldsymbol{E}_0\ , \tag{10}$$

where ε_p and ε_m are the relative permittivity of the particle and medium.

Particles also experience a force from the image charge induced at the surface of the dielectric layer, at a certain height (z_p) above the surface, can be calculated as follows:

$$\boldsymbol{F}_{image} = -\frac{q^2}{4\pi\varepsilon_0(2z_p)^2}\mathbf{n}, \tag{11}$$

where $\mathbf{n}$ is a normal vector pointing up perpendicular to the surface.

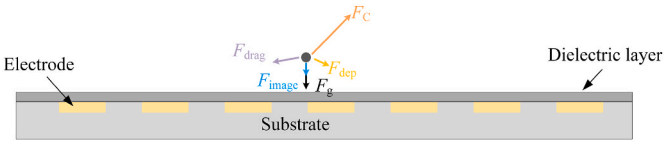

Fig. 16. Force diagram on single particle.

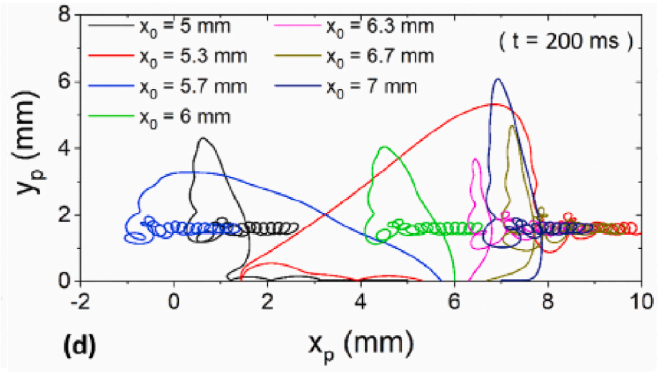

Fig. 17. Trajectories of particles with different departure positions (x_0 represents departure position) [34].

Particle motion on the transport system depends on the particle's physical properties and the imposed electric field. Experimentally, the total weight of particles can be measured by an electronic balance and the total charge of particles can be measured by an electrometer or Faraday cup. The electric field calculation method has been discussed and methods of simulating particle trajectories in that field is introduced in this section.

The simulation of particle motion in an ETW field can be divided into two categories: single particle simulation and multiple particle simulation. Single particle simulation is easier to implement and can qualitatively evaluate the effect of the forces acting on particles and the effect of different electric fields on particle motion modes. Multiple particle simulations that also consider particle collisions are closer to physical reality and therefore more useful for equipment design and operation quantitatively.

3.2.1. Single particle simulation

To simulate single particle movement, the following equations of motion need to be solved:

$$\begin{cases} m\dfrac{d^2x}{dt^2} = \sum F_i\ , \\ m\dfrac{d^2z}{dt^2} = \sum F_j\ , \end{cases} \tag{12}$$

where m represents mass of particle; x and F_i represent the displacement and forces in the horizontal direction; z and F_j represent the displacement and forces in the vertical direction.

David and coworkers [69] used Runge-kutta method in solving motion equations. As for the electric field calculation, they built a computer interface and users can choose from three different field solving methods: analytical method, numerical method, and a combination of numerical method and analytical method according to the user's accuracy acquirement. The simulation results showed that levitation height would be higher with the increase of voltage in curtain mode. And both simulation results and experimental results showed that particle's levitation height decreased with the increase of frequency [70].

Kawamoto and Hayashi [63] have performed simulations and experimental research on the basic mechanism of movement of single liquid drop and soft body. The pitch of the electrodes was 2 mm and the movement of particles of three diameters was researched experimentally: a) less than one pitch; b) between 1.5 and 2.5 pitches; c) larger than 3.5 pitches. For a type c, liquid drop, the positive and negative Coulomb forces tended to be similar due to its large size across three electrodes, so the electrokinetic effect on it was cancelled. As a result, a four-phase wave is more effective to move type c liquid drop than three-phase wave. A type b liquid drop was in a stationary polarization stage when the voltage was constant and only moved with the transition of voltage. A type a liquid drop was easier to transport due to its smaller

size. The moving direction of three types of liquid drop was explained using the schematic drawing of the polarity of electrodes along the direction of the traveling wave.

In order to optimise removal efficiency, Horenstein et al. [38] simulated the trajectories of single particle in an EDS. A Fourier expansion method was used to solve Laplace's equation. They divided the simulation time into n parts (Δt) and precomputed the electric field for each type of boundary condition at each time period. For each discrete time step, the vector sum of forces acting on the particle ($\sum F_n$) was calculated, then the acceleration, velocity (U) and displacement (dx) of the particles and for the vertical direction.

$$\begin{cases} dU = \left(\sum F_n \Big/ m\right)\Delta t, \\ dx = U\Delta t. \end{cases} \tag{13}$$

In addition, they assumed that when a particle contacts the EDS surface, its perpendicular velocity and parallel velocity retain 25% and 90% of the incoming value, respectively. Therefore, with the discrete time step method, the position of the particle can be calculated for the full-time scale. With this simulation method and in comparisons with experiments [39], they studied the effects of charge-mass ratio, particle radius, electrode spacing and starting positions on the particle movement. The key conclusions are that smaller particle tends to move more synchronously with the traveling wave and the initial position of a particle can lead to different chaotic trajectory.

Recently, Zouaghi and Zouzou [34] made similar simulations, but delved deeper into the theory of particle motion. They calculated the electric field using the same Fourier expansion method as Masuda et al. [9] and analysed the effect of the first and second harmonics of the traveling potential wave on particle motion:

$$\begin{aligned} V(x,z,t) &\approx W_{for} + W_{back} \\ &= V_0\left[\frac{3}{2}a_1 e^{-\frac{2\pi}{\lambda}z}\,\mathrm{Cos}\left(\frac{2\pi}{\lambda}x - \omega t\right) + \frac{3}{2}a_2 e^{-\frac{4\pi}{\lambda}z}\,\mathrm{Cos}\left(\frac{4\pi}{\lambda}x + \omega t\right)\right], \end{aligned} \tag{14}$$

Here V_0 is amplitude of the voltage on the electrodes, and a_1 and a_2 are the coefficients of first order and second order Fourier series based on their simulation model.

Zouaghi and Zouzou [34] also added the effects of the image-, DEP-, gravitational- and drag forces. Moreover, they ignored the thickness of the electrodes and dielectric barrier and assumed an elastic collision on the contact between particle and conveyor surface, which means that the particle's perpendicular velocity is reversed and parallel velocity remains constant. They divided the second order differential moving equation into four first order equations:

$$\begin{cases} v_x = \dfrac{dx}{dt}, \\ a_x = \dfrac{dv_x}{dt}, \\ v_z = \dfrac{dz}{dt}, \\ a_z = \dfrac{dv_z}{dt}, \end{cases} \tag{15}$$

where v_x and v_z are velocity in x and z direction, a_x and a_z are acceleration in x and z direction. Similar simplifying methods were used by Jie et al. [35].

Through analysing single particle trajectory under different simulation parameters, Zouaghi and Zouzou found that the initial position had a large effect on the initial of movement, but had little effect on the average velocity of the particle in steady state. The particles' trajectories with different departure positions are shown in Fig. 17. Backward motion was thought to be caused by backward harmonic waves. They concluded that analysing the effect on particle levitation height and displacement and optimising the frequency are necessary for EDS optimisation.

3.2.2. Multiple particle simulations and experimental research

Multiple particle simulation picture is quite different with single particle simulation scenarios [71]. In order to improve the understanding of particle motion and performance of particle separation using ETW, Adachi et al. [102] simulated multiple particles trajectories and compared the results with experiments. First, the potential distribution was calculated with the two-dimensional finite element method in a cyclic domain of the two-pitch width. Then, a series of force formulas involving electric field strength and particle parameters was presented. Finally, a three-dimensional modified hard-sphere model was introduced into the DEM simulation model, which takes the collision order between particles into account. A modified hard-sphere model has higher accuracy than hard sphere model and can significantly reduce computation time [72]. The motion equations were calculated using the Runge-Kutta method. Through the numerical results, the authors studied the effects of frequency and concluded that:

i. The direction of particle transport is related to the frequency of the applied voltage;
ii. Particles move synchronously with the traveling wave at low frequency;
iii. Some particles' velocities are slower than the traveling wave velocity at medium frequency;
iv. Most particles are transported backwards at relative high frequency and are not transported but only vibrated at very high frequency.

Moreover, Adachi et al. [102] predicted the particles' motion both in air and vacuum and illustrated the particles' motion and maximum height. The results indicated that particles would float higher in vacuum than in air. And in air, smaller particles, with relatively higher drag force, would not fly as high as larger particles.

Liu and Marshall [73] adopted a soft-sphere model to simulate multiple particles and research the effect of particle adhesion and collisions on motion modes. They considered soft-sphere model more realistic as the hard-sphere models are too fast for simultaneous collisions for a single particle. They used the boundary element method to calculate the electric field and decoupled it for a time-varying electric field. To reduce the computational cost, they used a box-particle multiple expansion method and dimensionless models. They introduced the "sweeping effect", in which synchronous moving particles could sweep forward low charge particles. Adhesion forces hindered the particle motion and affected particle's motion mode. They observed both forward and backward transport at high frequency, while forward-moving particles tended to have a higher charge. Finally, they claimed that higher charge particles lofted to higher altitudes, which may be utilized for the separation of particles.

Gu and coworkers [64] performed multiple particles simulations based on the Hertz-Mindlin contact model using DEM. The computational domain was restricted to 14.66 mm long (consisting of 12 electrodes) and the voltage was a four-phase square wave. The quantity of simulated particles was 10,000 and their size distribution and properties were consistent with lunar regolith simulant FJS-1. Detailed analyses for particle lifting from the conveyer surface was provided and the relationship between the particle's velocity and applied frequency was studied. The results showed that particles could get a higher backward transport rate at 1.04 m/s when the frequency was at 200 Hz, which was thought to be utilized in the transport of particles. The applied frequency and electrode configuration effect the particle's moving direction simultaneously. Experimental results within their designed platform showed that particles could also be transported backward at very low frequency, such as 2 Hz [65].

Digital printing technologies in electrophotography have also studied ETW theory for application to toner particles. Kober [75] researched

Table 3
Summary of selected prior research, collated in columns by research group.

Research Group		Kawamoto and coworkers [10,83,97,102]	Marshall and coworkers [73]	Zouaghi and Zouzou [27,34,67]
Charge of particles		Initial charge: 0.01~ −0.03 μC/g, increased with vibration to saturation	Mean value of charge: $-8.53\ 10^{-9}$ μC; Standard deviation: $9.22\ 10^{-9}$ μC	Most positively charged and the charge per gram was of the order of 0.01 μC/g.
Relationship between transport rate with	Voltage amplitude	Transport rate increased linearly with voltage (with a threshould voltage)	Only simulated with 1.6 kV	Particles velocity stagnated at a certain critical value
	Voltage type	Square wave was the most effective (RMS field strength)	Only simulated with square wave	Only used square wave; Traveling wave was more effective than Standing wave
	Electrode parameters	Particle was not transported if particle radius was 3.5 times larger than electrode separation	Width: 1 mm Separation: 2 mm; depth: 40 μm;	Small width/gap values decreased the ratio of particles moving backward
	Frequency	Transport rate increased with increasing frequency at low frequency	Not researched	20 Hz–100 Hz, average velocity continued to increase; above 100 Hz, average velocity droped with the increase of frequency
Relationship between Transport direction with	Frequency	Forward with low frequency; Backward with high frequency; Non-transport with extremely high frequency >250 Hz; Critical frequency is linked with particle size and electric field (which may be used to separate particle size)	At high frequency, particles transported both forward and backward.	At low frequency, particles moved forward. Over 50 Hz, a considerable amount of particles moved backward;
	Particle charge	Not researched	The forward-moving particles tended to have higher charge magnitude than moving the backward	High Q/M moved forward Lower Q/M particles moved backward
	Voltage	Not researched	Not researched	More particls moved backward at four-phase low voltage
Particle transport classified by Transport direction or mode		Forward and backward transport; Vibration mode	Hopping mode; Surfing mode	Forward: low frequency, high voltage, smaller size or high Q/M Backward: high frequency, low voltage value, big particles or low Q/M
Effect of particle collision and adhesion		Added in the simulation	High adhesion reduced transported particle; At medium frequency, particle collisions helped backward moving particles to move forward	Not researched
Levitation height		Decreased with increasing particle size	Increased with particle charge magnitude	Maximum levitation height increased with frequency at first and then decreased with further increase of frequency

the differences in motion between conductive and insulating toners. The conclusions are:

i. Insulating toner must be charged before it can be transported.
ii. The toner charging and the particle velocity mainly depend on the magnitude of the electric field intensity.
iii. Toner particles with smaller size and higher conductivity move faster and the critical frequency, at which particle's traveling direction reverses, is higher.

In contrast to the finding of Zouaghi and Zouzou [34] for single particle, Thompson [74] found that multiple particles behaviour was essentially independent of the initial particles' positions because the total electric field was not only generated by the traveling wave but also influenced by other charged particles and their image charges. This ensemble electric field may led to a self-consistent behaviour of multiple particles movement, in a large scale, which is not affected by the initial positions [74]. Taniguchi et al. [76] stated that mechanical vibration of the system could improve the driving characteristics.

Lunar soil particle transport and separation by size has been conducted by Kawamoto and coworkers [83, 85, 102], which is introduced in section 2.3.2. Kawamoto et al. [54] found experimentally that the maximum transport rate of lunar soil simulant FJS-1 was 13 g/min for an ETW conveyor with a width of 100 mm using mechanical vibration to assist particle transport. In the size separation system developed by Adachi et al. [102], particles smaller than 20 μm could be collected at 250 mm height and particles of about 10 μm could be collected effectively at 1.5 m height under vacuum. However, there was a trade-off between separation rate and collection, with a higher separation rate resulting in smaller collection amounts. The main cause was the accumulation of particles on the conveyor and the interaction between particles that hinder their movement. Testing the system must be performed under a high vacuum to avoid arcing at the voltages required for transport.

3.2.3. *Summary*

Table 3 summarises the major simulation and experimental studies of particle transport by ETW methods. Particle charge, transport rate, transport direction, transport mode, effect of particle collision and adhesion, and levitation height of particles have been researched.

There are four main findings:

1. The charge-to-mass ratio is affected by contact with the dielectric layer. After repeated contact, particles become saturated and the saturation charge is largely related to their physical properties.
2. The transport rate of particle is affected by voltage amplitude, voltage type (wave form and phase), electrode configuration parameters and frequency of voltage change. Larger voltage amplitude generates a larger electric field, thus increases particle transport rate.
3. The frequency of applied voltage is a critical parameter that influences particle transport rate and direction. Particles may move backward at higher frequencies. However, high frequency is ill-defined because different research groups use different experimental parameters and their conclusions about the boundary range of low and high frequency is different.

4. The levitation height of particle is affected by particle mass and charge. Collecting particles at different height can be used to separate particles.

4. Research gaps identified

4.1. Development needs

Simulation research methods allow a deeper understanding of the mechanism of particle transport in an ETW field. In recent years, multiple models and simulation methods have been applied to explore this transport theory. In spite of the large number of relevant simulations and experiments there is a lack of simple design rules that a designer could use to create a system to meet a stated set of design requirements.

The literature review has highlighted five key limitations in the existing research:

i. ETW is applied in widely diverse fields, including cell separation, dust mitigation of solar panels, lunar beneficiation and toner particle transport. This diversity weakens the integration between different lines of research and hinders the development and implementation of practical ETW systems.
ii. Motion of particles in an ETW system is affected by many parameters, such as voltage type, voltage frequency, electrode configuration, particle type. Different research groups use different experimental and simulation models, which leads to different conclusions at different scales.
iii. The comparison relationship between simulation and experimental results is not straightforward, making it difficult to reproduce and apply published models.
iv. The simulation process needs to be more rigorous. The accuracy of each step of simulation process needs to be evaluated, such as calculation of electric fields and the set up of particle motion simulation models. Many studies keep the particle charge constant during transport. However, triboelectric charging between particles and the dielectric layer must be included.
v. Realistic simulations need to be experimentally verified where both the simulation and the experiments involve multiple particles.

Experimental results involving multiple particles may show significant differences to single particle simulations [34]. Multiparticle simulations and experiments have only compared certain results such as general moving height [102], and require greater detail. Experiments can provide more direct and accurate information in the design and application of devices. Innovative design of experimental platforms, such as the configuration of experimental conveyors [87, 97], and additional mechanical and magnetic methods can be used to improve the performance and wider application [16, 88, 116, 119].

Particle motion in an electrostatic field is affected by a complex combination of factors. However, most conclusions in the literature are qualitative and the basic relationships between particle transport characteristics, conveyor parameters and applied voltage remain unclear. This makes experimentally observed phenomena difficult to explain and presents challenges in optimising equipment design. For example, the phenomenon that particles move backward at a relatively high frequency electric field is poorly understood, as is the different effects of dust loading by aerosol- and sieve deposition [36, 102].

Recently, the ETW system has gained more attention and many calculation methods and models have been proposed [37, 73, 101]. The combination of improved theoretical calculations and laboratory experiments will help better understand the physical mechanism of how particles move and interact in the ETW field.

4.2. Summary

The ETW method has undergone considerable development in recent years and has emerged as an innovative method for use in particle transport and separation. To improve its performance, several research gaps have emerged from this literature review:

i. Calculation of the electric field is critical to the development of robust models for the ETW system. Accurate and fast analytical solutions are not currently embedded in existing simulations, which largely rely on Fourier expansion methods and the finite element methods.
ii. The effect of frequency on particle motion, particularly with regards to backward motion, has not yet been explained thoroughly, which may become a bottleneck in the development of ETW, or may be exploited to separate particles by size.
iii. The effect of size and shape characteristics of the particles is often overlooked.
iv. Large scale simulations of multiple particles in an ETW field has not been carried out comprehensively; this is critical to design practical systems.
v. Experimental verification of multiple particles ETW flows needs to be carried out both to validate simulations but also allow the reliable specification of system parameters.
vi. Motion modes are complex, and the transition between modes requires greater investigation.

Declaration of competing interest

The authors declare that they have no known competing financial interests or personal relationships that could have appeared to influence the work reported in this paper.

Data availability

No data was used for the research described in the article.

Acknowledgment

The authors are grateful to the sponsors of Resource Geophysics Academy, Imperial College London, for supporting this research.

References

[1] A. Sayyah, M.N. Horenstein, M.K. Mazumder, G. Ahmadi, Electrostatic force distribution on an electrodynamic screen, J. Electrost. 81 (2016) 24–36.
[2] M. Mazumder, M.N. Horenstein, J.W. Stark, Peter Girouard, R. Sumner, B. Henderson, O. Sadder, I. Hidetaka, A.S. Biris, R. Sharma, Characterization of electrodynamic screen performance for dust removal from solar panels and solar hydrogen generators, IEEE Trans. Ind. Appl. 49 (2013) 1793–1800.
[3] C. Han, Q. Zhou, J. Hu, C. Liang, X. Chen, J. Ma, The charging characteristics of particle–particle contact, J. Electrost. 112 (2021), 103582.
[4] K.M. Abdelaziz, J. Chen, T.J. Hieber, Z.C. Leseman, Atomistic Field Theory for contact electrification of dielectrics, J. Electrost. 96 (2018) 10–15.
[5] A.E. Wang, P.S. Gil, M. Holonga, Z. Yavuz, H.T. Baytekin, R.M. Sankaran, D. J. Lacks, Dependence of triboelectric charging behavior on material microstructure, Physical Review Materials 1 (2017).
[6] S. Trigwell, N. Grable, C.U. Yurteri, R. Sharma, M.K. Mazumder, Effects of surface properties on the tribocharging characteristics of polymer powder as applied to industrial processes, IEEE Trans. Ind. Appl. 39 (2003) 79–86.
[7] S. Matsusaka, H. Maruyama, T. Matsuyama, M. Ghadiri, Triboelectric charging of powders: a review, Chem. Eng. Sci. 65 (2010) 5781–5807.
[8] F. Chowdhury, M. Ray, A. Sowinski, P. Mehrani, A. Passalacqua, A review on modeling approaches for the electrostatic charging of particles, Powder Technol. 389 (2021) 104–118.
[9] S. Masuda, M. Washizu, M. Iwadare, Separation of small particles suspended in liquid by nonuniform traveling field, IEEE Trans. Ind. Appl. 23 (1987) 474–480.
[10] H. Kawamoto, K. Seki, N. Kuromiya, Mechanism of travelling-wave transport of particles, J. Phys. Appl. Phys. 39 (2006) 1249–1256.

[11] J.R. Melcher, E.P. Warren, R.H. Kotwal, Theory for finite-phase traveling-wave boundary-guided transport of triboelectrified particles, IEEE Trans. Ind. Appl. 24 (1989) 7.

[12] F.W. Schmidlin, Modes of traveling wave particles transport and their applications, J. Electrost. 34 (1995) 20.

[13] F.B. Tatom, V. Srepel, R.D. Johnson, N.A. Contaxes, J.G. Adams, H. Seaman, B. L. Cline, Lunar Dust Degradation Effects and Removal or Prevention Concepts, NASA Technical Repor, NASA, 1967, p. 206.

[14] S. Masuda, Y. Matsumoto, Theoretical characteristics of standing-wave electric curtains, Electr. Eng. Jpn. 93 (1973) 13.

[15] M. Mazumder, R. Sharma, A.S. Biris, J. Zhang, C. Calle, M. Zahn, Self-cleaning transparent dust shields for protecting solar panels and other devices, Part. Sci. Technol. 25 (2007) 5–20.

[16] H. Kawamoto, T. Shibata, Electrostatic cleaning system for removal of sand from solar panels, J. Electrost. 73 (2015) 65–70.

[17] R.A. Sims, A.S. Biris, J.D. Wilson, C.U. Yurteri, M.K. Mazumder, C.I. Calle, C. R. Buhler, Development of a transparent self-cleaning dust shield for solar panels, in: IEEE Joint Meet. Electrostat, 2003, pp. 814–821.

[18] P.E. Clark, C.I. Calle, S.A. Curtis, J.F. Keller, F. Minetto, J.G. Mantovani, Electrostatic dust control on planetary surfaces, in: AIP Conference Proceedings, American Institute of Physics, 2007, pp. 400–406.

[19] P.E. Clark, S.A. Curtis, F. Minetto, J. Marshall, J. Nuth, C. Calle, SPARCLE: electrostatic dust control tool proof of concept, in: AIP Conference Proceedings, American Institute of Physics, 2010, pp. 549–556.

[20] fish 0,punct]">M. Mazumder, R. Sharma, A.S. Biris, M.N. Horenstein, J. Zhang, H. Ishihara, J.W. Stark, S. Blumenthal, O. Sadder, Electrostatic Removal of Particles and its Applications to Self-Cleaning Solar Panels and Solar Concentrators, William Andrew Publishing, 2011.

[21] A. Sayyah, M.N. Horenstein, M.K. Mazumder, Mitigation of soiling losses in concentrating solar collectors, IEEE, in: IEEE 39th Photovoltaic Specialists Conference (PVSC), IEEE, 2013, 0480-0485.

[22] A. Sayyah, M.N. Horenstein, M.K. Mazumder, A comprehensive analysis of the electric field distribution in an electrodynamic screen, J. Electrost. 76 (2015) 115–126.

[23] A. Sayyah, M.N. Horenstein, M.K. Mazumder, Performance restoration of dusty photovoltaic modules using electrodynamic screen, in: IEEE 42nd Photovoltaic Specialist Conference (PVSC), IEEE, 2015, pp. 1–3. IEEE.

[24] A.A.R. Bernard, R.I. Centra, E. Argentieri, R.S. Eriksen, S. Garner, MarkN. Horenstein, MalayK. Mazumder, Optimization of optical performance and dust removal efficiency of electrodynamic screen (EDS) films for improving energy-yield of solar collectors, in: 2018 IEEE 7th World Conference on Photovoltaic Energy Conversion (WCPEC)(A Joint Conference of 45th IEEE PVSC, 28th PVSEC & 34th EU PVSEC), IEEE, 2018, pp. 3451–3454. IEEE.

[25] A. Faes, D. Petri, J. Champliaud, J. Geissbühler, N. Badel, J. Levrat, B. Roustom, A. Hessler-Wyser, N. Wyrsch, C. Ballif, G.O. Getaz, G. McKarris, M. Despeisse, Field test and electrode optimization of electrodynamic cleaning systems for solar panels, Prog. Photovoltaics Res. Appl. 27 (2019) 1020–1033.

[26] M. Mazumder, C. Elinger, K. O'Connor, R. Eriksen, A. Bernard, M.N. Horenstein, J. Yellowhair, N. Joglekar, S. Garner, J. Bones, C. Morales, H. Acuña, Industrial production and field evaluation of transparent electrodynamic screen (EDS) film for water-free cleaning of solar collectors, in: 2019 IEEE 46th Photovoltaic Specialists Conference (PVSC), IEEE, 2019, pp. 3269–3276. IEEE.

[27] A. Zouaghi, N. Zouzou, Impact of spatial harmonic waves on dielectric particles displacement in standing and traveling wave electric fields, J. Electrost. 98 (2019) 25–33.

[28] B. Guo, B. Figgis, W. Javed, Measurement of electrodynamic dust shield efficiency in field conditions, J. Electrost. 97 (2019) 26–30.

[29] B. Guo, W. Javed, Y.S. Khoo, B. Figgis, Solar PV soiling mitigation by electrodynamic dust shield in field conditions, Sol. Energy 188 (2019) 271–277.

[30] A. Sayyah, D.R. Crowell, A. Raychowdhury, M.N. Horenstein, M.K. Mazumder, An experimental study on the characterization of electric charge in electrostatic dust removal, J. Electrost. 87 (2017) 173–179.

[31] M. Mazumder, M. Horenstein, J. Stark, D. Erickson, A. Sayyah, S. Jung, F. Hao, Development of self-cleaning solar collectors for minimizing energy yield loss caused by dust deposition, in: Proceedings of the ASME 2013 7th International Conference on Energy Sustainability, American Society of Mechanical Engineers, Minneapolis, MN, USA, 2013.

[32] M. Mazumder, M.N. Horenstein, N.R. Joglekar, A. Sayyah, J.W. Stark, A.A. R. Bernard, S.M. Garner, J.E. Yellowhair, H.Y. Lin, R.S. Eriksen, A.C. Griffin, Y. Gao, R.L. Centra, A.H. Lloyd, Mitigation of dust impact on solar collectors by water-free cleaning with transparent electrodynamic films: progress and challenges, IEEE J. Photovoltaics 7 (2017) 1342–1353.

[33] B. Guo, W. Javed, A. Al-Kuwari, Effect of voltage rise time on the efficiency of electrodynamic dust shield, IEEE J. Photovoltaics 9 (2019) 1086–1090.

[34] A. Zouaghi, N. Zouzou, Numerical modeling of particle motion in traveling wave solar panels cleaning device, J. Electrost. 110 (2021), 103552.

[35] Z. Jie, Z. Chuande, Z. Fuzhong, L. Shuhua, F. Miao, T. Yike, Experimental and numerical modeling of particle levitation and movement behavior on traveling-wave electric curtain for particle removal, Part. Sci. Technol. 37 (2018) 741–749.

[36] B. Guo, W. Javed, C. Pett, C.-Y. Wu, J.R. Scheffe, Electrodynamic dust shield performance under simulated operating conditions for solar energy applications, Sol. Energy Mater. Sol. Cell. 185 (2018) 80–85.

[37] J.K.W. Chesnutt, H. Ashkanani, B. Guo, C.-Y. Wu, Simulation of microscale particle interactions for optimization of an electrodynamic dust shield to clean desert dust from solar panels, Sol. Energy 155 (2017) 1197–1207.

[38] M.N. Horenstein, M.K. Mazumder, R.C. Sumner, J. Stark, T. Abuhamed, R. Boxman, Modeling of trajectories in an electrodynamic screen for obtaining maximum particle removal efficiency, IEEE Trans. Ind. Appl. 49 (2013) 707–713.

[39] M.N. Horenstein, M. Mazumder, R.C. Sumner, Predicting particle trajectories on an electrodynamic screen – theory and experiment, J. Electrost. 71 (2013) 185–188.

[40] A. Sayyah, R.S. Eriksen, M.N. Horenstein, M.K. Mazumder, Analysis of particle size distribution of residual dust in cleaning process using an electrodynamic screen, in: 2016 IEEE 43rd Photovoltaic Specialists Conference (PVSC), IEEE, 2016, pp. 2058–2060. IEEE.

[41] A. Sayyah, R.S. Eriksen, M.N. Horenstein, M.K. Mazumder, Performance analysis of electrodynamic screens based on residual particle size distribution, IEEE J. Photovoltaics 7 (2017) 221–229.

[42] C.E. Johnson, P.K. Srirama, R. Sharma, K. Pruessner, J. Zhang, M.K. Mazumder, Effect of particle size distribution on the performance of electrodynamic screens, in: 40th IAS Annual Meeting, 2005, pp. 341–345. IEEE.

[43] H.T. Ahmed, Z.M. Elmouloud, B. Ail, R. Ouiddir, A. Tilmatine, Experimental analysis of micronized plastic particle movement on electrodynamic screens, Int. J. Environ. Stud. 79 (2021) 72–87.

[44] W. Javed, B. Guo, Effect of relative humidity on dust removal performance of electrodynamic dust shield, J. Electrost. 105 (2020), 103434.

[45] A. Zouaghi, N. Zouzou, L. Dascalescu, Assessment of forces acting on fine particles on a traveling-wave electric field conveyor: application to powder manipulation, Powder Technol. 343 (2019) 375–382.

[46] J.N. Rasera, J.J. Cilliers, J.A. Lamamy, K. Hadler, The beneficiation of lunar regolith for space resource utilisation: a review, Planet. Space Sci. 186 (2020), 104879.

[47] H. Kawamoto, S. Kojima, Electrostatic precipitation in the martian environment, J. Aero. Eng. 32 (2019), 04019006.

[48] C.I. Calle, M.K. Mazumder, C.D. Immer, C.R. Buhler, S. Clements, P. Lundeen, A. Chen, J.G. Mantovani, Electrodynamic dust shield for surface exploration activities on the Moon and Mars, in: 57th International Astronautical Congress, 2006. A5-2.

[49] C.I. Calle, C.R. Buhler, J.G. Mantovani, S. Clements, A. Chen, M.K. Mazumder, A. S. Bins, A.W. Nowicki, in: Electrodynamic Dust Shield for Solar Panels on Mars, 35th Lunar and Planetary Science Conference, 2004, pp. 15–19.

[50] P. Atten, H.L. Pang, J.-L. Reboud, Study of dust removal by standing-wave electric curtain for application to solar cells on Mars, IEEE Trans. Ind. Appl. 45 (2009) 75–86.

[51] R. Sharma, C.A. Wyatt, J. Zhang, C.I. Calle, N. Mardesich, M.K. Mazumder, Experimental evaluation and analysis of electrodynamic screen as dust mitigation technology for future Mars missions, IEEE Trans. Ind. Appl. 45 (2009) 591–596.

[52] H. Kawamoto, M. Uchiyama, B.L. Cooper, D.S. McKay, Mitigation of lunar dust on solar panels and optical elements utilizing electrostatic traveling-wave, J. Electrost. 69 (2011) 370–379.

[53] H. Kawamoto, Improved electrostatic shield for lunar dust entering into mechanical seals of equipment used for long-term lunar exploration, in: 44th International Conference on Environmental Systems, 2014.

[54] H. Kawamoto, Electrostatic and Magnetic Cleaning Systems for Removing Lunar Dust Adhering to Spacesuits, 2012.

[55] N.A. Mohajer, C.-Y. Wu, R. Moore, N. Sorloaica-Hickman, Design of an electrostatic lunar dust repeller for mitigating dust deposition and evaluation of its removal efficiency, J. Aerosol Sci. 69 (2014) 21–31.

[56] C.I. Calle, C.R. Buhler, J.L. McFall, S.J. Snyder, Particle removal by electrostatic and dielectrophoretic forces for dust control during lunar exploration missions, J. Electrost. 67 (2009) 89–92.

[57] K.K. Manyapu, P. De Leon, L. Peltz, J.R. Gaier, D. Waters, Proof of concept demonstration of novel technologies for lunar spacesuit dust mitigation, Acta Astronaut. 137 (2017) 472–481.

[58] K.K. Manyapu, L. Peltz, P. De Leon, Self-cleaning spacesuits for future planetary missions using carbon nanotube technology, Acta Astronaut. 157 (2019) 134–144.

[59] C.I. Calle, J.L. McFall, C.R. Buhler, S.J. Snyder, E.E. Arens, A. Chen, M.L. Ritz, J. S. Clements, C.R. Fortier, S. Trigwell, in: Dust Particle Removal by Electrostatic and Dielectrophoretic Forces with Applications to NASA Exploration Missions, Proc. ESA Annual Meeting on Electrostatics, ESA, Minneapolis, MN, 2008.

[60] C.I. Calle, C.R. Buhler, M.R. Johansen, M.D. Hogue, S.J. Snyder, Active dust control and mitigation technology for lunar and Martian exploration, Acta Astronaut. 69 (2011) 1082–1088.

[61] J.R. Melcher, E.P. Warren, R.H. Kotwal, Traveling-wave delivery of single-component developer, IEEE Trans. Ind. Appl. 25 (1989) 6.

[62] J.R. Melcher, E.P. Warren, R.H. Kotwal, Theory for pure-traveling-wave boundary-guided transport of tribo-electrified particles, Part. Sci. Technol. 7 (1989) 1–21.

[63] H. Kawamoto, S. Hayashi, Fundamental investigation on electrostatic travelling-wave transport of a liquid drop, J. Phys. Appl. Phys. 39 (2006) 418–423.

[64] J. Gu, Q. Wang, Y. Wu, L. Feng, G. Zhang, S. Li, L. Tian, W. Yao, Numerical study of particle transport by an alternating travelling-wave electrostatic field, Acta Astronaut. 188 (2021) 505–517.

[65] J. Gu, G. Zhang, Q. Wang, C. Wang, Y. Liu, W. Yao, J. Lyu, Experimental Study on Particles Directed Transport by an Alternating Travelling-Wave Electrostatic Field, Powder Technology, 2022, p. 397.

[66] S. Masuda, K. Fujibayashi, K. Ishida, H. Inaba, Confinement and transportation of charged aerosol clouds via electric curtain, Electr. Eng. Jpn. 92 (1972) 10.

[67] A. Zouaghi, N. Zouzou, P. Braud, Study of dielectric particles motion in traveling and standing electrostatic waves using particle tracking velocimetry, J. Phys. Appl. Phys. 53 (2020).
[68] H. Kawamoto, N. Hasegawa, K. Seki, Traveling wave transport of particles particle size classification, Proceedings of Japan Machinery Society 69 (2003) 1216–1221.
[69] D. Hu, W. Balachandran, W. Machowski, Computer user interface and simulation for designing a travelling wave panel electrode, in: Proceedings of 1994 IEEE Industry Applications Society Annual Meeting, 1994, pp. 1621–1626.
[70] D. Hu, W. Balachandran, W.W. Machowski, Design of traveling-wave field panel for pharmaceutical powders based on computer simulation of particle trajectories, IEEE Trans. Ind. Appl. (1997) 33.
[71] Y.N. Gartstein, J.G. Shaw, Many-particle effects in travelling electrostatic wave transport, J. Phys. Appl. Phys. 32 (1999) 2176–2180.
[72] M. Adachi, Dynamics of Electromagnetic Particles and its Application for Mitigation and Utilization Technologies of Regolith on Moon, Mars, and Asteroids, Department of Applied Mechanics Research on Precision Engineering, Waseda University, Japan, 2017, p. 206.
[73] G.Q. Liu, J.S. Marshall, Effect of particle adhesion and interactions on motion by traveling waves on an electric curtain, J. Electrost. 68 (2010) 179–189.
[74] M.D. Thompson, Y. Gartstein, J.T. LeStrange, Aspects of Toner Transport on a Traveling Wave Device, NIP & Digital Fabrication Conference, Society for Imaging Science and Technology, 1999, pp. 262–265.
[75] R. Kober, Traveling Wave Transport of Conductive Toner Particles, NIP & Digital Fabrication Conference, Society for Imaging Science and Technology, 2000, pp. 736–739.
[76] K. Taniguchi, S. Morikuni, S. Watanabe, Y. Nakano, T. Sakai, H. Yamamoto, T. Yagi, Y. Yamanoto, in: Improved Driving Characteristics for the Toner Transportation System, NIP & Digital Fabrication Conference, Society for Imaging Science and Technology, 2000, pp. 740–742.
[77] R. Kober, in: Simulation of Traveling Wave Toner Transport, NIP & Digital Fabrication Conference, Society for Imaging Science and Technology, 2002, pp. 453–457.
[78] K. Taniguchi, H. Yamamoto, Y. Nakano, T. Sakai, S. Morikuni, S. Watanabe, A new technique for measuring the distribution of charge-to-mass ration for toner particles with on-line use, J. Imag. Sci. Technol. 47 (2003) 224–228.
[79] K. Adachi, S. Yamana, T. Nakamura, in: Development System by Toner Transportation Using Traveling Wave Electric Field, NIP & Digital Fabrication Conference, Society for Imaging Science and Technology, 2005, pp. 597–601.
[80] M. Maeda, K. Maekawa, M. Takeuchi, Simulation of traveling wave toner transport considering air drag, J. Imag. Sci. Technol. 51 (2007) 431–437.
[81] F.W. Schmidlin, A new nonlevitated mode of traveling wave toner transport, IEEE Trans. Ind. Appl. 27 (1988) 8.
[82] A.C. Yen, C.D. Hendricks, A planar electric curtain used as a device for the control and removal of particulate materials, J. Electrost. 4 (1978) 12.
[83] H. Kawamoto, K. Shirai, Electrostatic transport of lunar soil for in situ resource utilization, J. Aero. Eng. 25 (2012) 132–138.
[84] H. Kawamoto, K. Hata, T. Shibata, Vertical transport of lunar regolith and ice particles using electrodynamic traveling wave, J. Aero. Eng. 34 (2021).
[85] H. Kawamoto, Sampling of small regolith particles from asteroids utilizing an alternative electrostatic field and electrostatic traveling wave, J. Aero. Eng. 27 (2014) 631–635.
[86] H. Kawamoto, M. Kato, M. Adachi, Electrostatic transport of regolith particles for sample return mission from asteroids, J. Electrost. 84 (2016) 42–47.
[87] M. Adachi, H. Kawamoto, Electrostatic sampler for large regolith particles on asteroids, J. Aero. Eng. 30 (2017), 04016098.
[88] A. Tilmatine, A. Alibida, S. Zelmat, H. Louati, Y. Bellebna, F. Miloua, On the attraction force applied on metal pieces in a traveling wave conveyor, J. Electrost. 96 (2018) 64–68.
[89] S. Louhadj, N. Hammadi, S. Touhami, H. Louati, A. Hadjali, I.-E. Kimi, A. Tilmatine, Experimental analysis of the attraction force applied on metal particles using a double-side electrical curtain, J. Electrost. 105 (2020).
[90] X. Wang, X. Wang, F.F. Becker, P.R.C. Gascoyne, A theoretical method of electrical field analysis for dielectrophoretic electrode arrays using Green's theorem, J. Phys. Appl. Phys. 29 (1996) 1649–1660.
[91] H. Morgan, A.G. Izquierdo, D. Bakewell, N.G. Green, A. Ramos, The dielectrophoretic and travelling wave forces generated by interdigitated electrode arrays: analytical solution using Fourier series, J. Phys. Appl. Phys. 34 (2001) 1553–1561.
[92] N.G. Green, A. Ramos, H. Morgan, Numerical solution of the dielectrophoretic and travelling wave forces for interdigitated electrode arrays using the finite element method, J. Electrost. 56 (2002) 235–254.
[93] R. Cicchett, A. Faraone, On the optical behavior of the electromagnetic field excited by a semi-infinite electric traveling-wave current, IEEE Trans. Antenn. Propag. 53 (2005) 4015–4025.
[94] T. Sun, H. Morgan, N.G. Green, Analytical solutions of ac electrokinetics in interdigitated electrode arrays: electric field, dielectrophoretic and traveling-wave dielectrophoretic forces, Phys. Rev. E - Stat. Nonlinear Soft Matter Phys. 76 (2007), 046610.
[95] V. Gauthier, A. Bolopion, M. Gauthier, Analytical formulation of the electric field induced by electrode arrays: towards automated dielectrophoretic cell sorting, Micromachines (2017) 8.
[96] S. Masuda, M. Washizu, I. Kawabata, Movement of blood cells in liquid by nonuniform traveling field, IEEE Trans. Ind. Appl. 24 (1988) 217–222.
[97] H. Kawamoto, Some techniques on electrostatic separation of particle size utilizing electrostatic traveling-wave field, J. Electrost. 66 (2008) 220–228.
[98] W. Machowski, W. Balachandran, Dispersion and transport of cohesive lactose powder using travelling wave field technique, Powder Technol. 99 (1998) 251–256.
[99] H. Kawamoto, S. Naoto, Traveling wave transport of particles and particle size classification, J. Imag. Sci. Technol. 48 (2004) 404–411.
[100] W. Machowski, W. Balachandran, D. Hu, Influence of electrode geometry on transport and separation efficiency of powders using traveling wave field technique, in: IEEE Industry Applications Conference Thirtieth IAS Annual Meeting, 1995.
[101] J.K.W. Chesnutt, J.S. Marshall, Simulation of particle separation on an inclined electric curtain, IEEE Trans. Ind. Appl. 49 (2013) 1104–1112.
[102] M. Adachi, H. Moroka, H. Kawamoto, S. Wakabayashi, T. Hoshino, Particle-size sorting system of lunar regolith using electrostatic traveling wave, J. Electrost. 89 (2017) 69–76.
[103] H. Kawamoto, H. Morooka, H. Nozaki, Improved electrodynamic particle-size sorting system for lunar regolith, J. Aero. Eng. 35 (2022).
[104] S. Masuda, T. Kamimura, Approximate methods for calculating a non-uniform travelling, J. Electrost. 1 (1975) 351–370.
[105] L.C. Weiss, D.P. Thibodeaux, Separation of seed by-products by an AC electric field, J. Am. Oil Chem. Soc. 61 (1984) 886–890.
[106] Z. Dudzicz, The path of oscillation of dust particles in the field of the electric curtain of the plane type supplied with AC voltage, J. Electrost. 23 (1989) 207–214.
[107] Z. Dudzicz, Electrodynamics of charged dust particles and repulsion force within plane-type electric curtain, J. Electrost. 51 (2001) 111–116.
[108] Z. Dudzicz, E. Grządziel, Influence of the AC voltage frequency on the oscillation trajectory and path length of particles inside a planar–type electric curtain, J. Electrost. 77 (2015) 8–12.
[109] Z. Dudzicz, Confinement of charged dust particles by a hybrid-type electric curtain, J. Electrost. 70 (2012) 72–76.
[110] E. Grün, M. Horanyi, Z. Sternovsky, The lunar dust environment, Planet. Space Sci. 59 (2011) 1672–1680.
[111] M. Anand, I.A. Crawford, M. Balat-Pichelin, S. Abanades, W. van Westrenen, G. Péraudeau, R. Jaumann, W. Seboldt, A brief review of chemical and mineralogical resources on the Moon and likely initial in situ resource utilization (ISRU) applications, Planet. Space Sci. 74 (2012) 42–48.
[112] I.A. Crawford, Lunar resources: a review, Prog. Phys. Geogr. 39 (2015) 137–167.
[113] G.B. Sanders, W.E. Larson, Progress made in lunar in situ resource utilization under NASA's exploration technology and development program, J. Aero. Eng. 26 (2013) 5–17.
[114] M. Hecht, J. Hoffman, D. Rapp, J. McClean, J. SooHoo, R. Schaefer, A. Aboobaker, J. Mellstrom, J. Hartvigsen, F. Meyen, E. Hinterman, G. Voecks, A. Liu, M. Nasr, J. Lewis, J. Johnson, C. Guernsey, J. Swoboda, C. Eckert, C. Alcalde, M. Poirier, P. Khopkar, S. Elangovan, M. Madsen, P. Smith, C. Graves, G. Sanders, K. Araghi, M. de la Torre Juarez, D. Larsen, J. Agui, A. Burns, K. Lackner, R. Nielsen, T. Pike, B. Tata, K. Wilson, T. Brown, T. Disarro, R. Morris, R. Schaefer, R. Steinkraus, R. Surampudi, T. Werne, A. Ponce, Mars oxygen ISRU experiment (MOXIE), Space Sci. Rev. 217 (2021) 1–76.
[115] K. Hadler, D.J.P. Martin, J. Carpenter, J.J. Cilliers, A. Morse, S. Starr, J.N. Rasera, K. Seweryn, P. Reiss, A. Meurisse, A universal framework for space resource utilisation (SRU), Planet. Space Sci. 182 (2020), 104811.
[116] H. Kawamoto, Vibration transport of lunar regolith for in situ resource utilization using piezoelectric actuators with displacement-amplifying mechanism, J. Aero. Eng. 33 (2020), 04020014.
[117] D. Qian, J.S. Marshall, J. Frolik, Control analysis for solar panel dust mitigation using an electric curtain, Renew. Energy 41 (2012) 134–144.
[118] R. Pethig, Review article-dielectrophoresis: status of the theory, technology, and applications, Biomicrofluidics 4 (2010).
[119] H. Kawamoto, H. Inoue, Magnetic cleaning device for lunar dust adhering to spacesuits, J. Aero. Eng. 25 (2012) 139–142.